

Observations of Transiting Exoplanets with the James Webb Space Telescope (JWST)

Charles Beichman

*NASA Exoplanet Science Institute, California Institute of Technology, Jet Propulsion
Laboratory*

Bjoern Benneke, Heather Knutson, Roger Smith

California Institute of Technology

Pierre-Olivier Lagage

CEA, Saclay

Courtney Dressing, David Latham

Center for Astrophysics, Harvard University

Jonathan Lunine

Cornell University

Stephan Birkmann, Pierre Ferruit, Giovanna Giardino

European Space Agency

Eliza Kempton

Grinnell College

Sean Carey, Jessica Krick

Infrared Processing and Analysis Center, California Institute of Technology

Pieter D. Deroo, Avi Mandell, Michael E. Ressler, Avi Shporer, Mark Swain, Gautam

Vasisht

Jet Propulsion Laboratory, California Institute of Technology

George Ricker

Massachusetts Institute of Technology

Jeroen Bouwman, Ian Crossfield

Max Planck Institute of Astrophysics

Tom Greene, Steve Howell

NASA Ames Research Center

Jessie Christiansen, David Ciardi

NASA Exoplanet Science Institute, California Institute of Technology

Mark Clampin, Matt Greenhouse

NASA Goddard Spaceflight Center

Alessandro Sozzetti

Osservatorio Astronomico Di Torino

Paul Goudfrooij, Dean Hines, Tony Keyes, Janice Lee, Peter McCullough, Massimo

Robberto, John Stansberry, Jeff Valenti

Space Telescope Science Institute

Marcia Rieke, George Rieke

University of Arizona

Jonathan Fortney

University of California, Santa Cruz

Jacob Bean, Laura Kreidberg

University of Chicago

Drake Deming

University of Maryland

Loïc Albert, René Doyon

Université de Montréal

David Sing

University of Exeter

Received _____; accepted _____

Contents

1	Introduction	8
2	Key Science Opportunities	12
2.1	Transit and Secondary Eclipse Spectroscopy	13
2.1.1	Giant Planet Spectroscopy	13
2.1.2	Spectroscopy of super-Earths and mini-Neptunes	16
2.1.3	Terrestrial Planet Spectroscopy	18
2.2	Atmospheric Dynamics and Weather	20
2.2.1	Giant Planet Phase Curves	20
2.2.2	Super-Earth Phase Curves	21
2.2.3	Secondary Eclipse Mapping	22
2.2.4	Modeling Considerations	23
2.3	Transit Photometry	24
2.3.1	Thermal Emission of Nearby Earths	24
2.3.2	Transit Timing Variations	24
2.3.3	Known Transit Validation and Characterization	25
2.3.4	Searches for New Planets in Known Systems	25
3	Targets for <i>JWST</i> : Ground Surveys, Kepler, TESS, M Star Surveys, CHEOPS & GAIA	26

3.1	Desirable Target Characteristics	26
3.2	Surveys for New Targets	27
3.3	Expected Number of Targets	30
3.4	Characterizing Host Stars and Screening Candidates	31
3.5	Effects of Stellar Variability	32
3.6	Refining the Properties of Confirmed Planets	32
3.7	Determining When to Observe	33
4	Transit Best Practices	35
4.1	The Hubble Space Telescope (<i>HST</i>)	37
4.2	Kepler	38
4.3	The Spitzer Space Telescope	40
4.3.1	IRAC	41
4.3.2	IRS & MIPS Photometry	44
5	<i>JWST</i> Operations for Transits	45
5.1	Observatory Overview	45
5.2	Observatory Operations for Transit Science	49
5.2.1	Exposures Overview	49
5.2.2	Data Volume and Data Rates	50
5.2.3	Event Driven Operations	52

5.2.4	Observation Planning	53
5.2.5	Transit Timing	55
6	Detector Issues and Features	56
6.1	HgCdTe Detectors for NIRCcam, NIRISS and NIRSpec	56
6.2	MIRI Detectors	57
6.3	Efficient Detector Readout Scenarios and Bright Star Limits	59
6.4	Laboratory Tests of HgCdTe detectors for Transit Observations	61
7	Instrument Modes for Transits	62
7.1	NIRSpec	63
7.2	NIRISS	68
7.2.1	Instrument Overview	68
7.2.2	Suggested modes for transit work	69
7.2.3	Bright Star Limit	69
7.2.4	Target Acquisition and Pointing Requirements	70
7.2.5	Operational Limitations & Efficiency	71
7.2.6	Data Simulations	73
7.3	NIRCcam	75
7.4	MIRI	77
8	Illustrative Science Programs and Cross Instrument Opportunities	79

9 Engage the Community	82
9.1 Data Processing Challenges and Simulations	82
9.2 Obtaining Transit Observations Soon After Launch	84
10 Conclusions	86
11 Acknowledgements	90
A Meeting Agenda and Attendees	97
B Detector Operations	101
C Illustrative Science Programs	106

1. Introduction

The study of exoplanets is called out explicitly in NASA’s Strategic Plan¹ as one of NASA’s high level science goals: “*Objective 1.6*: Discover how the universe works, explore how it began and evolved, and search for life on planets around other stars.” The Strategic Plan calls out the James Webb Space Telescope (*JWST*) explicitly as a critical facility for studying exoplanets: “JWST will allow us to . . .study in detail planets around other stars.” The *JWST* project also cites exoplanet research among its most important goals²: “*The Birth of Stars and Protoplanetary systems* focuses on the birth and early development of stars and the formation of planets...*Planetary Systems and the Origins of Life* studies the physical and chemical properties of solar systems (including our own) and where the building blocks of life may be present.” Now, with the construction of *JWST* well underway, the exoplanet community is starting to think in detail about how it will use *JWST* to advance specific scientific cases.

Thus, a workshop on exoplanet transit opportunities with *JWST* is timely. The study of exoplanets by transits has become a mature subfield of exoplanetary science, and arguably the most exciting. Two developments have occurred almost simultaneously to make this so. First, the *Kepler* spacecraft completed a four-year transit survey mission which has revolutionized the study of exoplanets by obtaining high-precision, high-cadence, continuous light curves of ~150,000 stars, providing the first statistically significant determination of planet frequency down to objects the size of the Earth (Burke et al. 2014). Second, transit spectroscopy of individual nearby transiting planets using primarily the Hubble Space Telescope (*HST*) and the Spitzer Space Telescope have provided proof-of-principle that useful data on the composition of exoplanet atmospheres can be derived in this way, even

¹http://www.nasa.gov/sites/default/files/files/FY2014_NASA_SP_508c.pdf.

²<http://jwst.nasa.gov/science.html>

down to “super-Earths” with diameters less than three times that of the Earth (Kreidberg et al. 2014).

JWST will revolutionize our knowledge of the physical properties of dozens to possibly hundreds of exoplanets by making a variety of different types of observations. Here we focus on transits and phase curves; direct detection via coronagraphy was considered in a 2007 white paper (for all *JWST* white papers see <http://www.stsci.edu/jwst/doc-archive/white-papers>) and will be revisited in the near future.

JWST’s unique combination of high sensitivity and broad wavelength coverage enables the accurate measurement of transit and orbital parameters with high signal-to-noise (SNR). Most importantly, *JWST* will investigate planetary atmospheres, determine atomic and molecular compositions, probe vertical and horizontal structure, and follow dynamical evolution (i.e. exoplanet weather). It will do this for a diverse population of planets of varying masses and densities, in a wide variety of environments characterized by a range of host star masses and metallicities, orbital semi-major axes and eccentricities.³

The sensitivity of *JWST* over its wavelength range of 0.6 to 28 microns compared to other missions and ground-based facilities has been amply documented (<http://www.stsci.edu/jwst/science/sensitivity>) and *JWST*’s halo orbit around the Earth-Sun L2 point provides long, highly stable, uninterrupted observing sequences

³ Of particular interest for *JWST* will be small planets ($R < 2 - 4R_{\oplus}$) located at a distance from their host stars such that their equilibrium temperatures could be comparable to that of our Earth. The range of the so-called “Habitable Zone” has been argued over by many authors since its original definition (Kasting et al. 1993). We take an agnostic approach to this question, referring loosely to planets whose stellar insolation is comparable to that of our own.

compared with the ground or *HST*. *JWST*'s detectors are capable of much better than 100 parts per million (ppm) precision over time periods from hours to days. Its suite of four instruments and multiple operating modes provides a large range of choices in trading off spectral resolution (R between 4 -3000), photometric sensitivity, and observing time. Taken together, these characteristics will make *JWST*'s transit and eclipse observations the best method for characterizing exoplanet atmospheres in the foreseeable future.

While *JWST*'s instrument suite will be described in detail below (§7), we present a brief introduction here:

- NIRSpec is a highly versatile spectrometer covering the spectral range from 0.7 to 5 μm with spectral resolution options ranging from a $R\sim 100$ prism to gratings for $R\sim 1000$ and 2700 (§7.1). In addition to its multi-object capability and integral field unit, NIRSpec has a number of fixed slits, including one optimized for transit spectroscopy ($1.6'' \times 1.6''$).
- NIRISS has a variety of imaging and spectroscopy modes. Of particular interest for transit science is a grism mode (§7.2) covering wavelengths 0.6 to 2.5 μm with a spectral resolution of $R\sim 300$ -800. This grism has been optimized for transit spectroscopy using a cylindrical lens to broaden the spectrum to a width of 20-30 pixels to reduce inter-pixel noise and to improve the bright-star limit ($J\sim 7$ -8 mag).
- NIRCам has a suite of broad-, medium-, and narrow-band filters covering wavelengths from 0.7 to 5 μm (§7.3). By combining a fast sub-array readout mode with a defocusing lens, NIRCам will be capable of imaging transit host stars as bright as $K\sim 6$ mag. NIRCам also has a grism mode covering the 2.4-5 μm range at $R\sim 1700$ which, with a fast sub-array readout, can observe stars as bright at $K\sim 4$ mag.
- MIRI provides photometric, coronagraphic and spectroscopic capabilities between 5

and $28\ \mu\text{m}$ (§7.4). In addition to broad-band filters, MIRI has medium ($R\sim 70$) and high ($R\sim 1550\text{-}3250$) resolution spectroscopic modes covering this entire range. The saturation limit is $K\sim 6$ mag for imaging at $8\ \mu\text{m}$ and $K\sim 3\text{-}4$ mag for spectroscopy.

This white paper is based on a meeting held at Caltech in March of 2014, bringing together observers, modelers and *JWST* project personnel with the following goals:

- Identify key science cases for *JWST* transit observations.
- Improve the understanding of instrument capabilities among the scientists attending the meeting and, through this white paper, among the broader exoplanet community.
- Inform instrument teams, the Project and Space Telescope Science Institute about the particular requirements for maximum precision, e.g. cadence, astrometry, observation duration.
- Identify lessons learned from other facilities such as *HST*, *Kepler* and *Spitzer*.
- Identify precursor activities needed for observational planning and interpretation.
- Develop plans for near-term work to ensure optimum on-orbit performance, and to engage the wider exoplanet community to plan transit observations with *JWST*.

The white paper is organized along the structure of the meeting, with key science opportunities (§2) and target selection (§3) followed by sections on best practices for transits learned from other missions (§4) and *JWST* operational considerations specific to transits (§5). Detector issues and features and the modes of each *JWST* instrument relevant to transits are discussed in §6 and §7. Section §8 presents some illustrative science programs with an emphasis on cross-instrument capabilities. The challenges of data processing and community engagement are then considered (§9), and the paper concludes with a

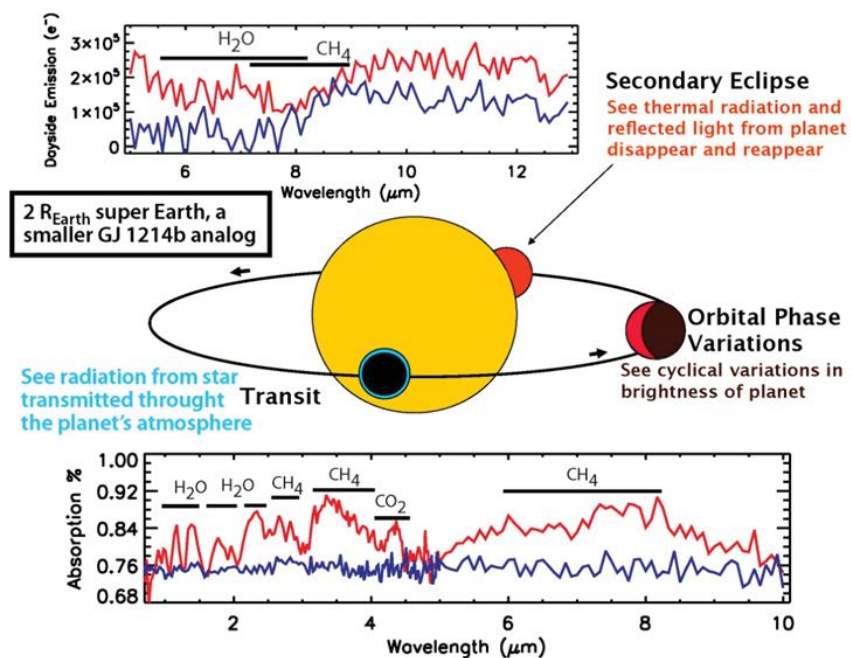


Fig. 1.— *Illustrative simulated spectra are shown for a smaller ($2.0 R_{\oplus}$) planet similar to GJ 1214b at that planet’s orbital location with the same host star. Primary (bottom) and secondary (top) transits are shown, and the planet model spectra were based on Fortney et al. (2013).*

summary of the most important findings (§10). Individual presentations at the Workshop go into much greater detail on these topics than can be given in this White Paper. These presentations are available on-line at the NASA Exoplanet Science Institute. Many of the section headings link directly to these presentations. The meeting agenda with live links (Appendix 1) and a list of attendees (Appendix 2) are given in the Appendix.

2. Key Science Opportunities

As a planet passes either in front of or behind its host star we detect either a “primary transit” or a “secondary eclipse” (Figure 1). In the former case we see stellar light filtered

through a thin annulus of the upper atmosphere of the planet. While primary transit signals are relatively insensitive to the vertical structure of the atmosphere, the measurements sample only a few scale heights in the upper atmosphere which may not be representative of the atmosphere as a whole. In the case of a secondary eclipse we directly detect radiation emitted by the star-facing side of the planet from which we can retrieve both atmospheric temperature structure and more fully representative chemical abundances. The figure also shows that it is possible to follow a planet throughout its orbit to measure its phase curve from which one can infer important information on the planet’s albedo (in reflected light) and its horizontal temperature structure (in thermal emission). In this section we address science opportunities for spectroscopy of gas and ice giant planets ($\sim 0.05 - 5M_{Jup}$, §2.1.1), Super Earths ($\sim 5 - 15M_{\oplus}$, §2.1.2) and even terrestrial-sized planets ($\sim 1 - 5M_{\oplus}$, §2.1.3 and 2.3.1). *JWST* will also investigate the dynamical processes of weather through the study of phase curves §2.2.

2.1. Transit and Secondary Eclipse Spectroscopy

2.1.1. Giant Planet Spectroscopy

With *JWST* transit spectroscopy we will address fundamental questions about gas and ice giant planets, putting their present-day characteristics into the context of theories of their formation and evolution. For example, to what extent is metal enrichment a hallmark of giant planets? How does a planet’s composition vary as a function of planet mass and migration history, stellar type and metallicity and, in particular, stellar C/O ratio (Öberg et al. 2011). By determining the abundances of key molecules (Figure 2, Shabram et al. (2011)a) we can begin to address these and other issues.

Today’s knowledge of the spectroscopy of exoplanets is roughly at the same level as

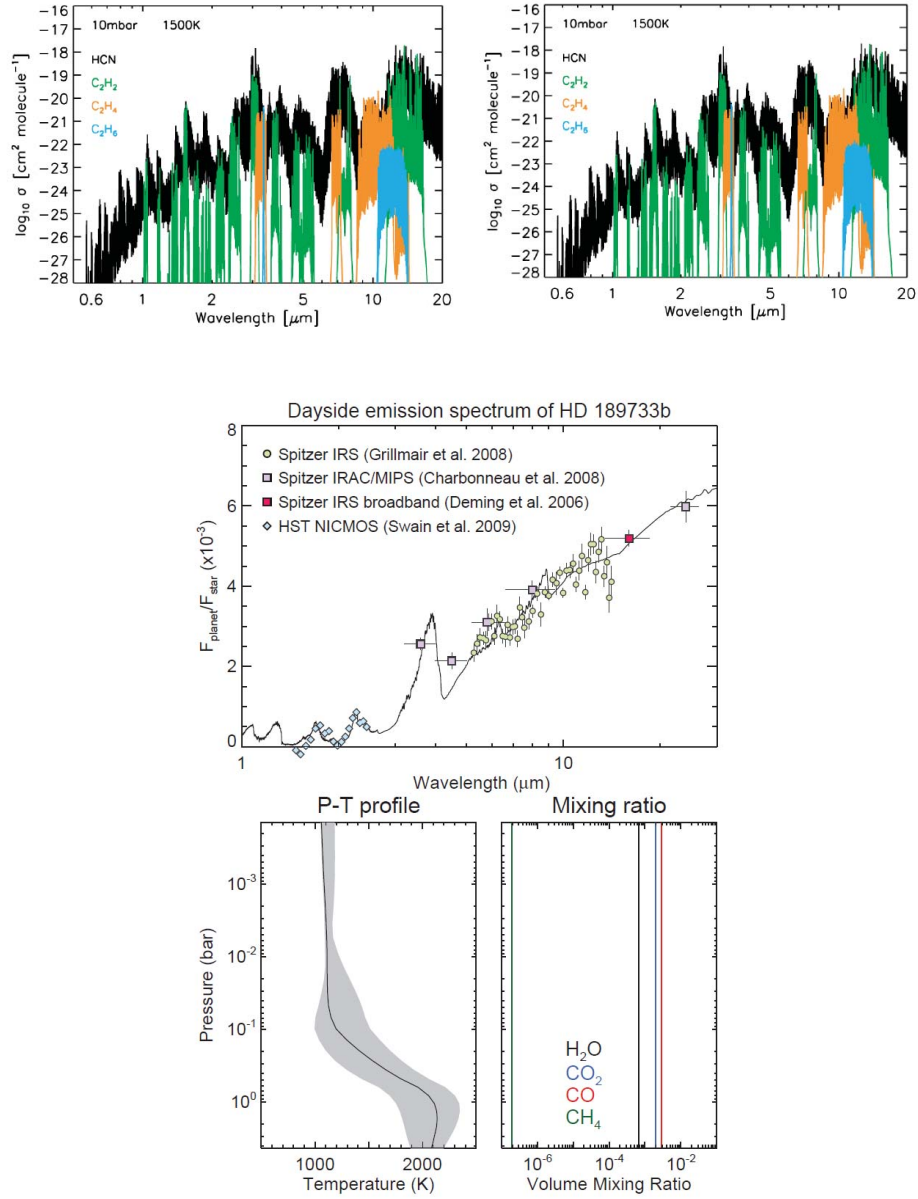


Fig. 2.— top) Model abundances for a $1 M_{Jup}$ planet at $1500 K$ (Shabram et al. 2011); bottom) Early observations of the transmission and emission spectra of HD189733b from Spitzer and HST have been inverted to yield Pressure-Temperature profile of the atmosphere along with mixing ratios of H_2O , CO_2 , CO, and CH_4 (Lee et al. 2012). (Fortney (2014), this workshop).

we had about the planets in our solar systems 50 years ago when, for example, it was determined that Jupiter’s atmosphere had a strong temperature inversion with CH_4 as a primary absorber (Gillett et al. 1969). As spectroscopic observations of exoplanets become available from *HST* and *Spitzer*, we are beginning to gain a comparable level of knowledge (Figure 2b; Lee et al. (2012)). However, with *JWST*’s high signal-to-noise ratio (SNR) at multiple wavelengths and high resolution we will obtain a much better characterization of the atmospheres of exoplanets, including vertical structure, elemental and molecular abundances, surface gravity, and the effects of non-equilibrium and/or photochemistry (Madhusudhan et al. 2014; Line & Yung 2013).

By examining elemental abundances through a broad survey of gas and ice giants covering a wide range of planet mass ($0.05 < M < 5M_{Jup}$), stellar metallicity ($-0.5 < [Fe/H] < 0.5$) and stellar spectral type (F5V-M5V), it will be possible to improve our understanding of the primary factors in the formation of massive planets. For example, an enhanced C/O ratio compared to the host star’s might be indicative of a core accretion formatino mechanism(Madhusudhan et al. 2014; Konopacky et al. 2013). Lowering the mass range to $0.03 M_{Jup}$ ($10 M_{\oplus}$) would reach into the realm of mini-Neptunes and Super-Earths (§2.1.2). Extending the mass range up to $10 M_{Jup}$ would provide an interesting comparison with low mass brown dwarfs to investigate whether there are compositional fingerprints of a different formation scenario. Recent progress with observations taken with *HST*/WFC3 is encouraging about what *JWST* will be able to accomplish with its greater collecting area and broader range of wavelengths. Figure 3 shows how the combination of *HST* transmission spectra and *Spitzer* emission photometry constrain the temperature profile of WASP-43b (Kreidberg et al. 2014).

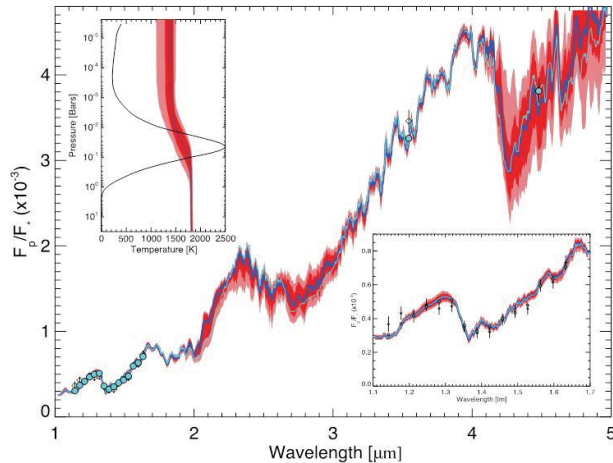


Fig. 3.— Recent, high precision observations of the emission spectrum of WASP-43b from *Spitzer* and *HST* have been inverted to yield Pressure-Temperature profile of the atmosphere. (Fortney (2014), this workshop). (Kreidberg et al. 2014).

2.1.2. Spectroscopy of super-Earths and mini-Neptunes

“Super Earths” or “mini-Neptunes” can be defined loosely as planets with a range of 5-15 M_{\oplus} . Results from *Kepler* suggest that such planets are very common (Petigura et al. 2013; Dressing & Charbonneau 2013), especially around late K and early M stars. On-going surveys with *Kepler*/*K2* will investigate this trend for still later spectral types. It is, however, striking that no “Super-Earth” exists in our own solar system, making their study in other planetary systems all the more exciting. The bulk properties of “Super-Earths” are quite diverse with some objects having large radii and low masses whereas others have comparable masses but much smaller radii and thus higher densities (Figure 4a). Large low-density super-Earths with large atmospheric scale heights will typically be easier to observe, both in transit and secondary eclipse phase. However, the highly interesting small, high-density super-Earths with potentially Earth-like properties require a substantial investment of *JWST* time in order to build up reasonable SNR (Batalha et al. 2014). This

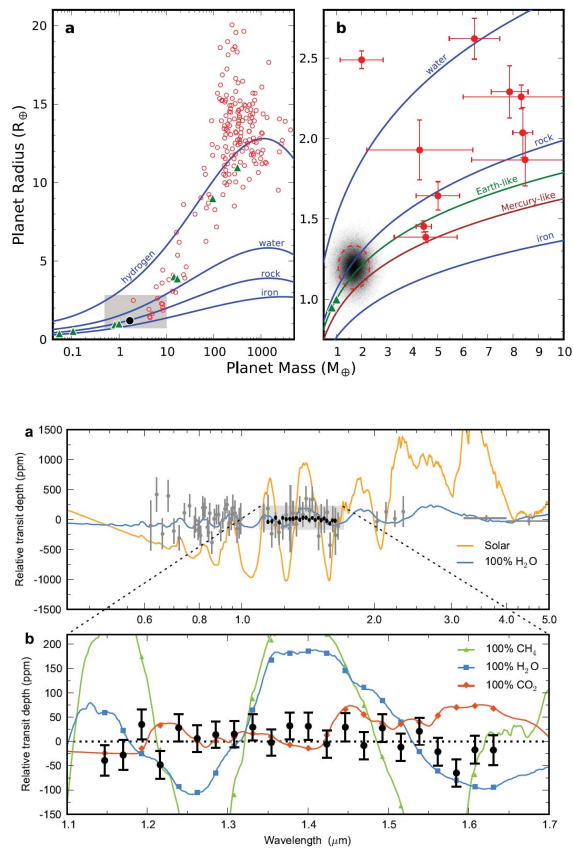


Fig. 4.— *Top, left)* The distribution of exoplanets across the full range of mass and radius. Solar system planets are denoted as green triangles. *top, right)* A close-up of planets with masses less than $10 M_{Jup}$ showing a range of bulk densities ranging from predominantly water and volatile rich to dense, rocky-iron bodies. The shaded area corresponds to the likely properties of Kepler-78b (Howard et al. 2013). *bottom)* HST observations of the spectrum of GJ 1214b with ~ 25 ppm precision (Kreidberg et al. 2014) along with various theoretical models none of which provide a particularly good fit to the data. One possible interpretation for the relatively flat spectrum is the presence of clouds or photochemical haze. (Kempton (2014), this workshop; (Kreidberg et al. 2014)).

trade-off in terms of time investment vs. scientific return will need to be confronted when planning observing strategies aimed at characterizing this group of planets.

The prototype for this class of object is GJ1214b, a planet with a mass of $6.6 M_{\oplus}$, radius of $2.7 R_{\oplus}$ and density of 1.9 g cm^{-3} orbiting an M3 star at a distance where its equilibrium temperature is approximately 550 K (Charbonneau et al. 2009). This object has been the target of numerous spectroscopic investigations but there remains fundamental uncertainty as to its nature, either a “mini-Neptune” composed primarily of a rock/ice interior with a large hydrogen dominated atmosphere and traces of water and methane, or a true “water world” with a predominantly icy interior and an H_2O atmosphere (Rogers & Seager 2010). *HST*/WFC3 spectroscopy of GJ1214b does not constrain its atmospheric composition, showing definitive evidence for a high-altitude, optically thick cloud or haze layer (Kreidberg et al. 2014). A similarly puzzling result holds for a second Super-Earth, HD 97658b, which also has a flat spectrum across the 1-1.8 μm region. In both cases, the presence of high altitude clouds or photochemical haze has been suggested as the origin for the relatively featureless spectra at these wavelengths. Alternatively, a high mean molecular weight atmosphere with low hydrogen abundance remains a viable alternative interpretation for HD 97658b. *JWST* observations spanning at least the 1-10 μm region may offer our first glimpse through the clouds as they become transparent at longer wavelengths.

2.1.3. Terrestrial Planet Spectroscopy

Terrestrial-sized planets can be defined as objects with a range of $1\text{-}5 M_{\oplus}$. Batalha et al. (2014) have made simulations of transit spectra obtained after observing 25 transits with NIRSpec for 1, 4 and $10 M_{\oplus}$ planets at a variety of equilibrium temperatures (Figure 5). The Hydrogen-rich atmospheres have a large scale height and are thus detectable over a broad range of temperatures and distances whereas the Hydrogen-poor atmospheres are barely detectable at the closest distances and hottest temperatures. These simulations suggest that it will be nearly impossible to measure spectra of terrestrial analogs (H-poor,

low scale height atmospheres) for all but the closest systems without a very large investment of dedicated telescope time.

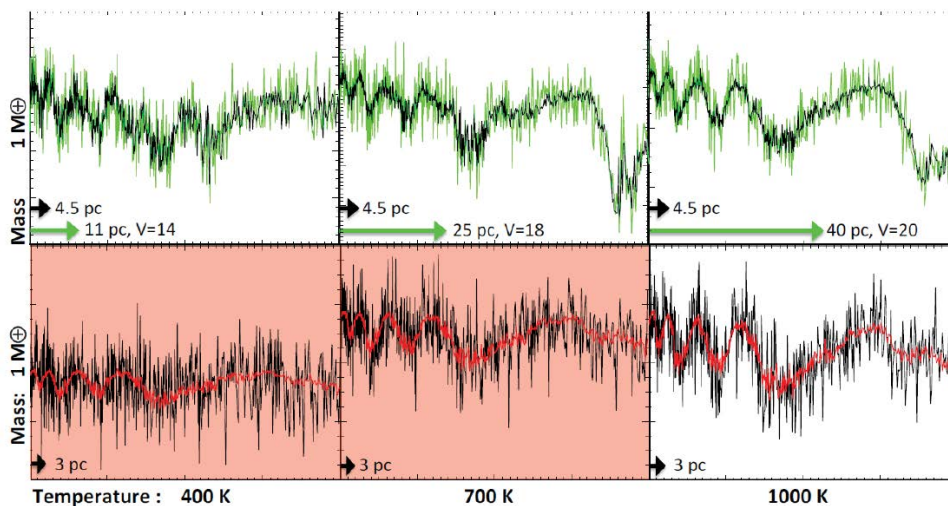


Fig. 5.— *Predictions for the detectability of the 1-5 μm spectra of a $1 M_{\oplus}$ planet using JWST to observe 25 primary transits. The planet is assumed to orbit an M star like GJ1214 and to have any of three equilibrium temperatures and two different atmospheric types (top, Hydrogen-rich; bottom, Hydrogen-poor). The simulations include a wide variety of noise sources (Batalha et al. 2014). In the H-rich case, the black lines indicate the simulated observations for a star at 4.5 pc while the green lines indicate the simulated spectra for different limiting distances. In the H-poor case, the red lines denote the model and the black lines the observations for a star at 3 pc. Temperature/mass combinations shaded in red have low SNR (<15) and may be challenging to interpret. (Kempton (2014), this workshop).*

2.2. Atmospheric Dynamics and Weather

2.2.1. Giant Planet Phase Curves

Transiting planets are usually found close to their host stars, because the probability of a transit is inversely proportional to the semi-major axis of the planetary orbit. The strong stellar tidal force experienced by planets in close orbits drives the planetary rotation to be synchronous with orbital revolution (Guillot et al. 1996). Synchronous rotation implies that, for a circular orbit, the star-facing hemisphere of a planet is constantly irradiated, while the anti-star hemisphere is perpetually dark. Strong zonal winds re-distribute energy longitudinally, mediated by radiative cooling of the atmosphere, leading to longitudinal infrared brightness gradients. Using infrared photometry, the most basic aspect of zonal thermal structure that we can detect is the day-night temperature difference. The existence and phase offset of localized hot spots is also inferred from the phase curve (Figure 6; Knutson et al. (2007)). Using rotational inversion techniques, the spatial resolution that can be obtained in longitude is intrinsically limited to about 5 cycles per planetary circumference (Cowan & Agol 2008). Nevertheless, significant insight can be obtained into the chemistry and dynamics of giant exoplanet atmospheres at that resolution, especially if spectroscopy can be obtained as a function of orbital phase. Photometric observations of hot Jupiter phase curves have been made with *Spitzer*, but *JWST* will be able to acquire spectroscopy across a broad range of wavelengths simultaneously. Only *JWST* will have the capability to acquire spectroscopy of multiple molecules at good SNR over the full exoplanet orbit. Time-resolved, multi-molecule spectroscopy will be informative concerning non-equilibrium chemical and thermal processes that can potentially play a major role in the atmospheric dynamics of close-in giant planets.

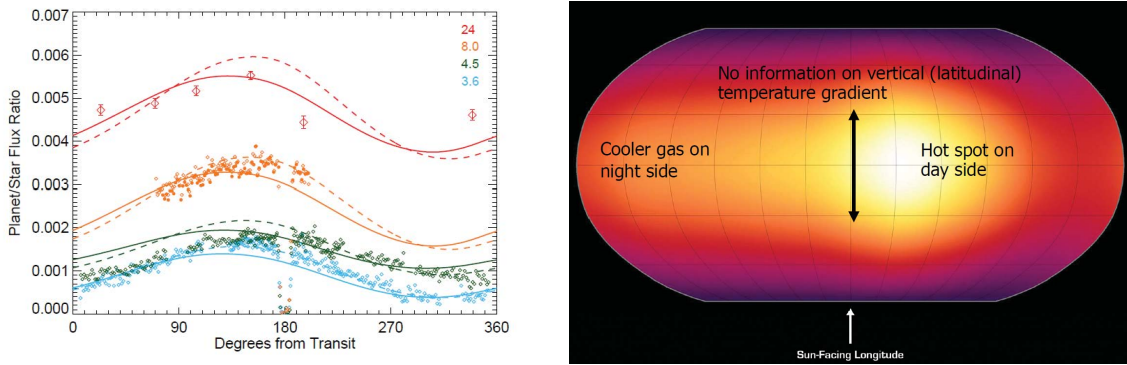


Fig. 6.— Multi-wavelength *Spitzer* observations through an entire orbit of the planet HD 189733b yield a thermal phase curve that can be used to infer properties of the planet’s atmosphere. left) Data at different wavelengths are plotted along with atmospheric circulation models using different amounts of metallicity (Knutson et al. 2012), solar (solid) and $5\times$ solar (dashed). right) A reconstructed map of the distribution of temperature across the surface of the planet suggests that supersonic winds shift the hottest gas away from the sub-stellar point (Knutson et al. 2007). (Knutson (2014), this workshop).

2.2.2. Super-Earth Phase Curves

Phase curve observations of super-Earths and mini-Neptunes are of particular scientific interest. A tidally-locked rocky planet that lacks an atmosphere will have a high contrast phase curve, with minimal heat transfer from the star-facing to anti-stellar hemisphere. The amplitude of the phase curve can be compared to the depth of the secondary eclipse in order to determine how much heat transfer is occurring (Knutson et al. 2007). Significant longitudinal heat transfer is not expected in the absence of an atmosphere, hence rocky planet phase curves can be used to establish that an atmosphere exists (Seager & Deming 2009). *Spitzer* has been able to place some rough limits on rocky planet phase curves (Seager & Deming 2009), but there are no definitive phase curve measurements from *Spitzer* for super-Earths. With JWST’s $6\times$ increased SNR due to its larger mirror diameter,

we estimate that *JWST* will be able to measure the broad-band phase curves of hot super-Earths and mini-Neptunes down to $\leq 4 R_{\oplus}$.

2.2.3. Secondary Eclipse Mapping

Beyond phase curves, *JWST* will be able to use a technique now being pioneered by *Spitzer*, wherein the photometric structure of secondary eclipse light curves at ingress and egress can be inverted to map the disk of the planet. The scale height of stellar atmospheres is about two orders of magnitude smaller than the radii of hot Jupiter exoplanets, hence the stellar limb resolves the star-facing hemisphere of the planet during ingress and egress at secondary eclipse. When the impact parameter is near zero, the limb of the star scans the planet approximately parallel to circles of longitude. In that case, secondary eclipse mapping gives the longitudinal temperature structure of the exoplanetary disk, but little to no latitude information (Williams et al. 2006). Longitudinal structure includes the phase offset of the hottest point due to advection by zonal winds (Knutson et al. 2007). In the case where the impact parameter differs significantly from zero, the stellar limb scans the planet at two oblique angles, that differ at ingress and egress. In this case, secondary eclipse mapping (Majeau et al. 2012a; de Wit et al. 2012a) can also provide latitude information. The slow rotation of tidally-locked hot Jupiters causes their zonal jets to be broad in latitude compared to Jupiter in our Solar System (Menou et al. 2003). The broadness of the jets facilitates spatial mapping, by making it easier to resolve that structure on the exoplanetary disk.

2.2.4. *Modeling Considerations*

Modeling will have to make significant advances to keep up with improvements in the observations. For example, we need to verify that different atmosphere models, which seek to fit physical and chemical parameters, e.g. pressure-temperature profiles and chemical abundances, yield consistent results when presented with identical physical assumptions and data. A valuable test of the community’s analysis methods would be to verify that multiple groups can retrieve the same atmospheric parameters from benchmark simulated datasets. Additionally, we must ensure that our conclusions are statistically robust (in a Bayesian sense) when compared with other physical interpretations (Hansen et al. 2014).

We must also examine model assumptions. Perhaps the most important thing is to consider how realistic it is to use one dimensional models to represent hemisphere-averaged conditions. A related issue is how significant patchy clouds are in affecting observations during transit and secondary eclipse. Clouds are now understood to be very important in the appearance of the brown dwarf siblings of exoplanets and probably in the spectra of Super-Earths as well (Figure 4b; Morley et al. (2014)). Further explorations of the conditions under which clouds and hazes emerge in the giant planet and super-Earth contexts are definitely needed. Progress can be made on several of these model validation issues by making use of observed spectra of brown dwarfs and directly imaged planets that sample temperature ranges similar to transiting planets.

Another modeling challenge results from the limited availability of opacity data in the temperature and pressure range appropriate for exoplanet atmospheres. To properly interpret spectroscopic observations, an accurate understanding of the relevant molecular and atomic opacities is required. While there are publicly available databases for this purpose, e.g. HITRAN and ExoMol, there are known deficiencies in these databases such as a reliable formulation of near-IR and optical methane opacities.

2.3. Transit Photometry

2.3.1. Thermal Emission of Nearby Earths

Simple calculations suggest that broadband MIRI photometry at 10-15 μm would be able to detect the secondary eclipse of a 300-350 K, 1 R_{\oplus} planet orbiting a nearby late M dwarf like GJ1214. In a single 45 minute transit the SNR at 15 μm would be ~ 0.5 -1, taking into account both stellar and zodiacal noise and a noise floor of 50 ppm. Observing 25 transits would result in a positive detection at the 3 to 5 σ level. In the more favorable cases of a system at 10 pc or closer, a target star of even later spectral type, or a lower noise floor of 25 ppm, it might even be possible to detect the broad spectral line of CO_2 at 15 μm . But this would be a very challenging project at the limit of *JWST*'s prowess and would require the detection by *TESS*, *Kepler*/*K2* or other transit survey of an appropriate target (§3.2).

2.3.2. Transit Timing Variations

Gravitational perturbations between planets in a multi-planet system can alter individual transit times by readily observable amounts. These deviations from simple orbits enable mass determinations for planets whose stellar Doppler reflex is unmeasurable and has been demonstrated in multi-planet *Kepler* systems (Lissauer et al. 2013). *JWST* could extend the temporal baseline for *Kepler* systems to over a decade for greatly improved parameter estimation and could make new measurements for *TESS* planets. Simple photometric observations would suffice to accomplish this goal, but the nature of the planetary system would have to be scientifically compelling in order to justify the *JWST* time.

2.3.3. *Known Transit Validation and Characterization*

Simple photometry of transits (as opposed to secondary eclipses) can be valuable because the atmospheric opacity of the planet may vary with wavelength, allowing multi-wavelength observations to probe the composition of the atmosphere. *Spitzer* photometry has played an important role in the initial characterization of bright transiting systems and *JWST* may play a similar role especially for systems too faint for more detailed spectroscopy.

A second reason to observe transits in the infrared is to validate transits as being due to genuine planets and not false-positive signals such as an eclipsing binary composed of small stars or a triple system with a much brighter star. While most systems observed with *JWST* will already be well characterized, there may be compelling faint M star targets observed with TESS, for example, needing a simple validation step showing that the transit signal is indeed achromatic. Infrared transit observations using *Spitzer* have been a valuable tool to eliminate false-positives in the *Kepler* data (Ballard et al. 2011). For scientifically compelling exoplanetary systems such as a habitable super-Earth transiting a nearby M-dwarf star, *JWST* could potentially help to eliminate false-positives while constraining the composition of the atmosphere.

2.3.4. *Searches for New Planets in Known Systems*

The photometric precision that can be achieved using space-borne platforms has numerous applications in exoplanetary science. Among these is the search for transits of additional planets in systems that are already known to host transiting planets. Space-borne searches of this type are warranted when the detection would be of great scientific importance and the transits that are being sought are beyond the sensitivity

of ground-based photometry. Such searches are most efficient when conducted using an observatory that has the capability to observe a given exoplanetary system for long uninterrupted periods of time, i.e. not occulted by the Earth. For example, *Spitzer* was used to search for a habitable planet in the GJ 1214 system (Fraine et al. 2013; Gillon et al. 2014) and also detected two sub-Earth-sized planet candidates around GJ 436b (Stevenson et al. 2012). *JWST* would be able to conduct a similar search for Earths and super-Earths in the habitable zones of nearby M-dwarf stars, provided that the specific case is scientifically compelling.

3. Targets for *JWST* : Ground Surveys, Kepler, TESS, M Star Surveys, CHEOPS & GAIA

In order to maximize the scientific yield from *JWST* planet observations, the community must plan ahead to select a well-vetted sample of planets. In this section we discuss desirable target system properties, sources of targets for *JWST*, the importance of measuring host star properties, initial vetting procedures for likely targets, and observation timing.

3.1. Desirable Target Characteristics

Observations of transits, eclipses and phase curves with *JWST* will yield the highest signal-to-noise for targets with these characteristics: bright, photometrically stable host stars; large ratio of planet to star radius; large atmospheric absorbing areas, driven by high planet temperature, low planet surface gravity, and low mean molecular weight of planetary atmospheres for transmission spectroscopy; deep spectral absorption features; relatively high planet to star temperatures for emission observations; and short orbital periods for

phase curves (less than a few days for reasonable observation times).

These observational considerations are often times at odds with each other (e.g., bright, small, and photometrically stable host stars) and are frequently inconsistent with the most scientifically interesting systems (e.g., small, cooler planets). As explained in the following section, new survey facilities are expected to produce significant numbers of interesting new targets: both small and large planets around mostly small, nearby stars. Many are expected to be in or near habitable zones, with semi-major axes large enough to reduce the effect of stellar insolation on the planetary atmospheres.

3.2. Surveys for New Targets

Many of the hot Jupiters that have already been detected with ground-based surveys and studied with *HST* are prime targets for *JWST*, but the smallest planets observable with *JWST* have most likely not yet been discovered. Small planets are interesting but challenging targets due to their smaller transit depths, but the challenge can be reduced by targeting smaller stars. The transit depth scales as the inverse square of the stellar radius, so the signal of a $2 R_{\oplus}$ planet around a $0.2 R_{\odot}$ late M dwarf is comparable to the transit depth of a gas giant around a Sun-like star. While the final SNR for such a system depends on the stellar radius, the orbital period, and the number of transits observed, the SNR advantage of studying planets orbiting small stars is very significant.

Several ground-based transit surveys are now targeting bright, low-mass stars to find planets with reasonable transit depths. MEarth (Nutzman & Charbonneau 2008; Berta et al. 2012) began monitoring the northern sky with eight 40-cm telescopes in 2008 and recently expanded to the southern sky with an additional eight telescopes. The KELT (Siverd et al. 2009) and HATNET (Bakos et al. 2011) surveys are continuing to find

interesting systems. The APACHE Project (Sozzetti et al. 2013) has started a survey from the Alps in 2012 and SPECULOOS (Gillon et al. 2013) will begin operations in the Atacama Desert in 2015. The Next Generation Transit Survey project (NGTS)⁴ will build on the success of its predecessor Super-WASP to search stars brighter than $V=13$ mag looking for Neptune-sized objects. The MASCARA survey will find several dozen planets around stars with $V < 8$ (Snellen et al. 2012).

From space, K2 (Howell et al. 2014) is likely to detect several hundred small planets orbiting bright stars. Although most of the stars observed during the prime *Kepler* mission were fainter than $V = 13$ mag, a large fraction of K2 targets will be brighter than $V = 12$. Based on the initial testing for the K2 mission, K2 should find roughly $50 \leq R_{\oplus}$ planets orbiting M dwarfs per year. After completion of its roughly 2.5-yr mission, K2 will have observed 10 times as much area on the sky as Kepler. For a uniform population of M stars, this corresponds to an average brightness increase of over 1.5 mag compared with Kepler. And since both the brightest M stars and the latest known M stars in each field are being targeted, one can always get lucky.

Larger K2 planets will also be interesting. K2’s 75 day observing period will find planets with much less insolation than the currently known hot Jupiters orbiting, on average, stars brighter than the average *Kepler* star. These large planets will produce strong signals when they transit their host stars, enabling high signal-to-noise characterization observations with *JWST*. It is possible that dozens of these candidates will have measured RV masses or sensitive mass upper limits by the time of the *JWST* launch. *Because K2 targets are being observed, validated and characterized as this document is being written, K2 will be an important source for both large and small new targets for observation by JWST early in the mission lifetime.*

⁴<http://www.ngtransits.org/index.shtml>

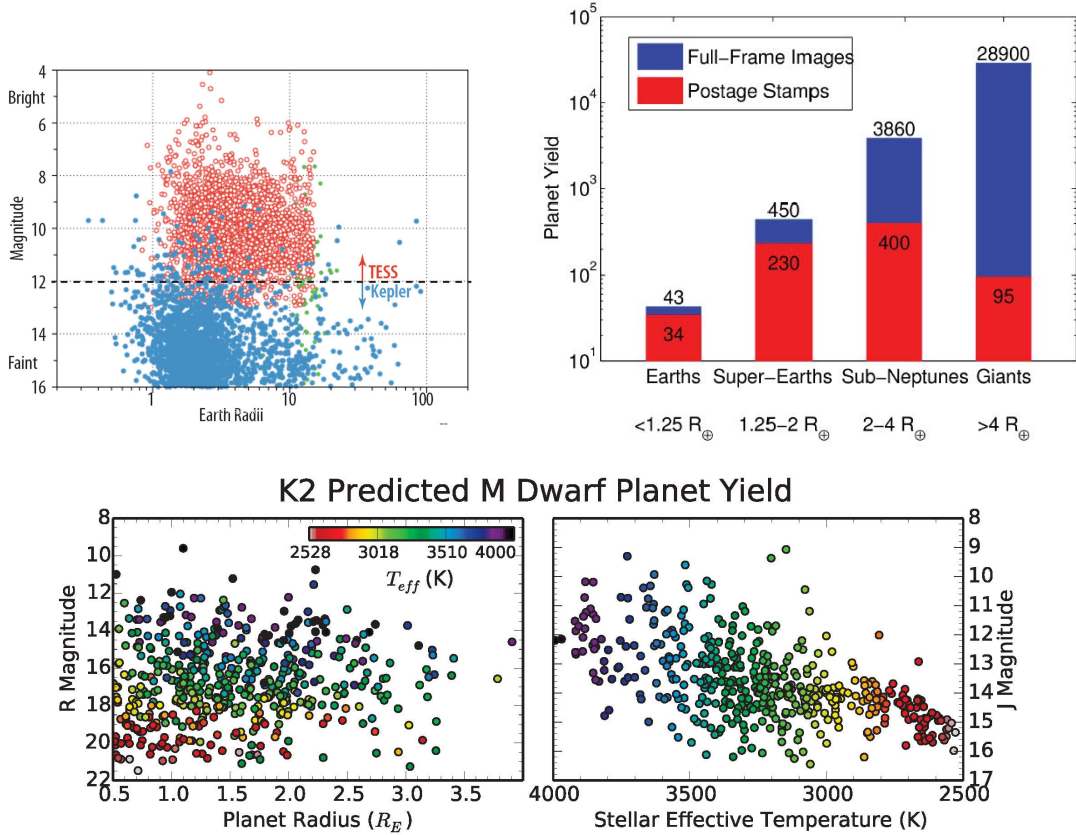


Fig. 7.— *top, left*) The planets detected by *TESS* (red) will typically be 5 magnitudes brighter than those found by *Kepler* (blue) thus making them excellent targets for *JWST* (Ricker et al. 2014). *top, right*) A histogram showing the distribution of planet sizes expected to be found by *TESS*, either in the full frame images or in postage stamps selected for closer examination (Sullivan et al. 2014). (Ricker (2014), this workshop). *bottom*) Predicted *R*- and *J*-band magnitudes of planet-bearing *M* dwarf stars found by the *Kepler/K2* survey as a function of planet radius (left) and stellar effective temperature (right; Crossfield, private comm.).

In later *JWST* observing cycles, the most important source of targets for *JWST* will be the all-sky *TESS* survey (Ricker et al. 2014). The majority of *TESS* targets will be bright stars, $V < 12$ mag (Figure 7). *TESS* yield simulations (Sullivan et al. in prep) suggest that *TESS* will detect approximately 40 Earth-size planets and 340 Super-Earths

during the course of the two-year survey. Roughly 20 of these small planets are expected to lie in or near the habitable zones of their host stars and a quarter of the small, habitable zone planets are likely to lie within the *JWST* continuous viewing zone. *TESS* will have good sensitivity to Super-Earths around early- to late-type M stars which *JWST* will be able to characterize in detail. A few verified *TESS* planets may be known at the time of the *JWST* launch, with significant numbers confirmed with mass measurements after the first couple years of *JWST* operations. *The timely validation and characterization of K2, TESS and other survey targets will require a significant investment in precision radial velocity measurements and adaptive optics imaging.*

3.3. Expected Number of Targets

The yield predictions for *TESS* and K2 are based on planet occurrence rates estimated from the results of the *Kepler* mission (Fressin et al. 2013; Dressing & Charbonneau 2013; Petigura et al. 2013) and the census of nearby stars. The RECONS survey (Henry et al. 2006) has cataloged the population of stars within 10 pc and determined that 75% of nearby stars are M dwarfs. Supplementing the sample of stars within 10 pc with additional catalogs of stars with known parallaxes (van Altena et al. 1995; Perryman et al. 1997; Lépine 2005; Dittmann et al. 2014) and assuming planet occurrence rates from Dressing & Charbonneau (2013) reveals that there should be approximately 80 transiting planets within 20 pc. Roughly ten of those planets are likely to be potentially rocky planets orbiting within the habitable zone with the closest system located within 9 ± 3 pc and orbiting a star as bright as $J \sim 5.5 \pm 0.9$ mag (Dressing et al., *in prep*).

It must be noted that these estimates are based on as yet incomplete processing of all of the *Kepler* data and may be optimistic (Foreman-Mackey et al. 2014), particular for the latest spectral types where *Kepler* data are sparse. Improved *Kepler* analysis followed by

results from *K2* and finally *TESS* will be critical to refining these estimates and, of course, identifying the best targets. To the extent that one of these planets is orbiting a late type M star with a correspondingly deep transit signal, it may be possible to characterize this planet in some detail, although at the expense of a large amount of *JWST* time to cover 25 or more transits (Figure 5).

3.4. Characterizing Host Stars and Screening Candidates

Planetary mass and radius estimates are directly tied to stellar properties. Accordingly, our knowledge of planetary properties is constrained by our knowledge of the host star. Prior to devoting *JWST* time (or even ground-based follow-up resources) to observing a planet it is crucial to characterize the host star. The parallaxes provided by Gaia (Perryman et al. 2001) will be useful for constraining the distances and absolute magnitudes of host stars. Coupled with ground-based spectra, those distance measurements should constrain the metallicities, temperatures, radii, and surface gravities of potential target stars.

In addition to obtaining spectra to refine the properties of the host star, we will also require high-resolution images in order to search for nearby stars and properly account for transit signal contamination. In some cases, a signal that initially appears to be a small planet transiting a single star may actually be caused by a background eclipsing binary, an eclipsing binary physically bound to the target star, a larger planet transiting a star in a binary star system or a larger planet transiting a background star (Brown 2003). Obtaining high-resolution imagery to rule out such blended systems is particularly important for determining the radii of planets detected by satellites with large pixels such as *Kepler*, *K2*, and *TESS*.

3.5. Effects of Stellar Variability

For targets that pass the initial screening tests, we will also need to examine the variability of the host star. Stars that exhibit large amplitude brightness variations due to spots may be challenging targets for transit or phase curve measurements. Secondary eclipse measurements are less affected by variability which evolves on a much slower timescale than the duration of the eclipse.

Starspots can greatly complicate the interpretation of transit data as a planet scans across a mottled stellar surface, changing the apparent depth of a transit from its true value or producing a flux change if the planet itself occults a starspot. (Pont et al. 2013; Huitson et al. 2013). JWST’s multi-wavelength capabilities can help to disentangle these effects as the contrast between a starspot and its star decreases to longer wavelengths.

3.6. Refining the Properties of Confirmed Planets

Planetary masses and radii must be determined before assessing a system’s suitability for *JWST* observations. Precision radial velocity (RV) measurements (or transit timing variations) confirm that an object is real and yield critical information needed for interpreting *JWST* spectra. The amplitude of the expected atmospheric signal depends the surface gravity of the planet, making knowledge of planetary mass and radius crucial when selecting which targets to observe.

Visible light spectrometers, including Keck/HIRES, HARPS, HARPS-N, the Lick Automated Planet Finder (APF) and VLT/ESPRESSO (on-line in 2016), will provide critical RV data. An advantage of TESS’s targets is that they will 3-5 magnitudes brighter than Kepler’s which will allow spectrometers on smaller telescopes to play a key role in follow-up programs (Figure 7). *NASA should make it a high priority to ensure ready access*

by the US community to appropriate RV capabilities.

As discussed in §3.1 and 3.2, many of the best planets for *JWST* will orbit M dwarfs. Due to their red colors, M dwarfs are faint in the optical bands traditionally used in radial velocity observations. However, M dwarf spectra contain considerable velocity information in the red optical and near-infrared. For instance, Bean et al. (2010) have achieved 5 m s^{-1} precision on late M dwarfs using CRIRES with an ammonia cell on the VLT. While promising, that precision is not sufficient for measuring the masses of potentially habitable Earths. However, the next generation of fiber-fed red optical and near-infrared spectrographs is expected to reach 1 m s^{-1} precision. CARMENES (Quirrenbach et al. 2012), HPF (Mahadevan et al. 2010), Spirou (Artigau et al. 2011), and Maroon-X⁵ are expected to begin operations in 2017 and should be able to provide mass estimates for the population of small planets that will be detected by transit surveys of bright stars.

The most promising *JWST* targets could be observed by the targeted (non-survey) CHEOPS satellite (Broeg et al. 2013) for better transit data to refine radius and bulk density determinations. CHEOPS is scheduled to be launched in 2017 and is expected to achieve a precision of 20 ppm over 6 hours for G-type stars with $V < 9$. The well-vetted planets with precisely measured masses and radii could even be observed with HST to obtain lower S/N spectra, to prescreen for relatively featureless transmission spectra obscured by clouds.

3.7. Determining When to Observe

One of the most basic requirements for conducting transit and secondary eclipse measurements is knowing when to expect events. For systems without observed transit

⁵<http://astro.uchicago.edu/~jbean/spectrograph.html>

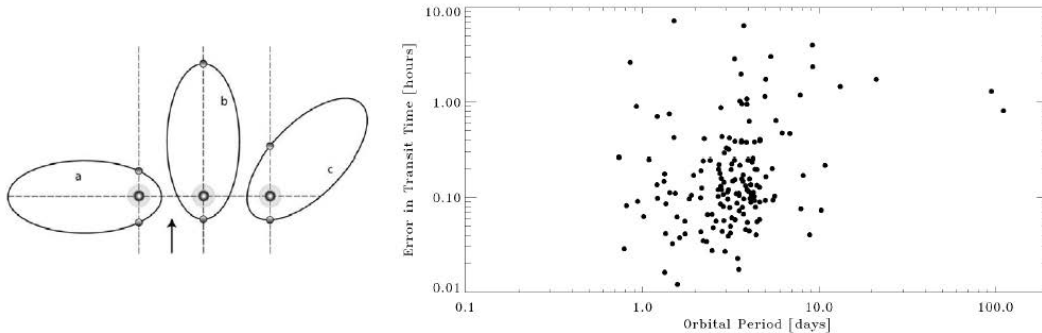


Fig. 8.— *left) The geometry of primary and secondary transits is shown for different orbital configurations. Determining the exact timing for a secondary transit requires detailed radial velocity observations. When the planet’s eccentricity and/or longitude of periastron are unknown or poorly known, the uncertainty in the secondary eclipse can be hours or even days. right) The uncertainty in future transit times in 2018 for a sample of transiting systems based on extrapolations from present day uncertainties in the parameters of simple Keplerian orbits. A few systems will have uncertainties as large as one hour or more by 2018, highlighting the need for continuing monitoring to update orbital information through the lifetime of JWST (Ciardi (2014), this workshop)*

timing variations, the typical precision of measured transit times and periods is sufficient to estimate the timing of primary transits to within $\ll 1$ hour out to mid 2018 (Figure 8). But for many systems and for later observing epochs it will be important to update orbital information before investing large amounts of *JWST* time.

Predicting secondary eclipses is challenging due to the uncertainty in the planet’s eccentricity and longitude of periastron. For planets originally detected via transit, a significant number of radial velocity measurements will be required to constrain the eccentricity and orientation of the system. In many cases, the secondary eclipse might not even be detected in the original photometry. While careful analysis of high SNR transit data may constrain these orbital parameters (Dawson et al. 2014), important K2

and *TESS* targets observed over only a few periods will have poorly determined orbital parameters without ground-based follow-up. *A continuing program of precision radial velocity monitoring to ensure precise timing of both primary and secondary transits is essential.*

If its operations continue beyond 2014, *Spitzer* would be the best observatory for searching for secondary eclipses for existing and newly-discovered planets. In addition, the success of ground-based studies of the secondary eclipses of hot Jupiters (Croll et al. 2011), suggests that such observations will be able to track the ephemerides of *TESS* and K2 planets with transit depths as shallow as $\sim 10^{-3}$.

4. Transit Best Practices

Many of the transit science opportunities described §2 will be challenging even for *JWST*. Over the last decade we have amassed a wealth of experience with space-based transit observations from *HST*, *Spitzer* and *Kepler*. All of these have achieved photometric precision of a 20-30 ppm with the careful design and execution of the observations and substantial post-processing. However, with *JWST*, we will not have the same baseline (17 years for STIS on *HST* and 10 years for *Spitzer*) for developing and refining the ideal observing strategies. Therefore it behooves us to examine the best practices and lessons learned from these missions, in order to begin the first cycle of *JWST* as well prepared as possible. Here we briefly describe the systematic sources of error which have been identified as contributing significantly to the quality of the photometric precision; the three recurring themes are thermal stability, pointing stability and electronic artifacts. The systematics and the suggested mitigation strategies, where available, are summarised in Table 1.

Systematic	Impact on photometry	Timescale	Frequency	Suggested mitigation
HST				
Thermal breathing	<2% ramp in flux time series, and offset first orbit	30 minutes	Every orbit	Detrend in processing
Electronics	Offset in first exposure per orbit	Length of exposure	Every orbit	Take a short first exposure and remove
Kepler				
Pointing tweaks	Discontinuities in flux time series	<30 minutes	Sporadically	Isolate pointing management timescales from scientific timescales of interest
Seasonal thermal changes	Ramps in flux time series	90 days	~Yearly	Detrend in processing
S/c pointing thermal changes	Ramps in flux time series	~2 days	~Monthly	Detrend in processing
Heater cycle thermal changes	Correlated noise in flux time series	3–6 hourly	Continuously	Isolate heater management timescales from scientific timescales of interest
Electronics	Correlated noise in flux time series and cross-contamination	Various	Continuously	Robust detector characterisation before launch
Reaction wheel zero crossings	Additional noise (<2%) in flux time series	0.01–0.5 days	Sporadically	Avoid zero crossings during times of scientific interest (ingress/egress/etc)
Spitzer IRAC				
Pointing wobble and pointing drift	Correlated noise in flux time series	0.08'' in 30–60 minutes, and 0.3''/day	Continuously	Build well understood gain maps
Electronics	1–10% ramp up (charge trapping?), and ~10% ramp down (persistence?)	1–24 hours (flux-dependent)	Per target	Robust detector characterisation before launch
Spitzer MIPS/IRS				
Pointing absolute offsets	2% discontinuity in flux	Each frame	Each frame	Avoid dithering
Flatfield errors	0.2% correlated noise in flux	1–3 hours	Continuously	
Electronics	2% ramp up in flux time series, 0.2% fallback in flux time series, and <2% latents (bright/dark)	2–10 hours, 10–30 hours, Hours–days	Start of observations, After ramp up saturates, Sporadically	Robust detector characterisation before launch
Artificial background variations	0.2% discontinuity in flux	Constant within AOR	Each AOR	

Table 1: Summary of systematic effects, their impacts and suggested mitigation strategies by spacecraft.

4.1. The Hubble Space Telescope (*HST*)

HST is a 2.4-m telescope in a low-Earth orbit. Launched in 1990, it has hosted several instruments spanning from the near-UV to the near-IR. For transit observations, some of the notable instruments have been STIS, the Near Infrared Camera and Multi-Object Spectrometer (NICMOS), the Advanced Camera for Surveys (ACS) and the Wide Field Camera 3 (WFC3).

Due to its 96-minute orbit, the thermal environment of the telescope is highly variable. The thermal breathing of the telescope, due largely to day/night temperature changes, causes changes in the focus over the duration of the observations. When generating a flux time series on a given target, this results in a ramp in the photometry which is highly repeatable from orbit to orbit. These ramps are common across multiple instruments in the focal plane. The first orbit in a set of observations on a given target typically experiences a different form of the ramp, and the standard observing procedure to offset this is to schedule an additional orbit at the start of the observations which is then discarded or deweighted. Due to the repeatable nature of the ramp in subsequent orbits, a standard common-mode systematic removal model has been developed to remove the thermal breathing.

An additional systematic that has been noted is the trend for the first exposure in each orbit to be offset from the remainder of the exposures. This is potentially attributable to electronics, and the current strategy is to take a short exposure at the beginning of each orbit which is then discarded.

Recent efforts to improve the photometric precision in transit observations have concentrated on the new scanning mode with the WFC3 instrument (Figure 3). By scanning the target Point Spread Function (PSF) across the CCD during the exposure, the total exposure time can be increased without saturation, improving the observing efficiency. The improvement in signal-to-noise from the additional photons arguably outweighs the

errors introduced by the varying inter- and intra-pixel sensitivities sampled during the exposure, but this is still being actively investigated.

Data analysis strategies for removal of systematic trends in HST transit and eclipse spectroscopic data have focused on removing repeatable and common-mode trends through self-calibration. The common trends in each orbit, usually attributed to thermal breathing of the telescope (see Table 1), can be removed by using data from before and after the transit/eclipse event to create a template which is then be divided out from all the orbits. This method is commonly called *divide-out* (Berta et al. 2012), but has been used in similar applications as well. Additionally, trends that are common in either the temporal dimension (such as the stellar spectrum and the sensitivity function) or the wavelength dimension (e.g. common-mode flux variations) can be removed by creating a template spectrum or a template light curve and then subtracting it (Deming et al. 2013; Mandell et al. 2013).

4.2. Kepler

The *Kepler* mission launched a 0.95-m optical telescope in 2009 into an Earth-trailing orbit, with the goal of obtaining very high precision photometry on 150,000 stars in a 100 square degree field of view in the constellation Cygnus. The prime mission ended in May, 2013 after the failure of its second reaction wheel, but NASA has recently approved plans to continue using the telescope for high precision time domain science in the ecliptic plane (Howell et al. 2014).

Kepler's orbit is much more thermally stable than *HST's*. A yearly cycle as the spacecraft orbits the Sun produces a common mode effect for all stars across the focal plane and is removed in detrending. Additionally, the spacecraft pointed toward Earth every month to download the accumulated data, and it took approximately two days after

the spacecraft returned to the science field for the temperature to settle back down to the seasonal average. This effect resulted in ramps of up to a few percent in the flux time series over those two days. In the early months of the mission, the reaction wheel heaters cycled every 3 to 6 hours, manifesting itself as a sinusoidal variation in the flux time series. While the mechanism of the coupling between the reaction wheel heaters and the focal plane were not understood, changes were made to the flight software to decrease the cycle period and amplitude to below a single observation (~ 30 minutes), which largely eliminated this effect. *Ideally, thermal management timescales should be well isolated from scientific timescales of interest* (1–30 minutes for transit ingress and egress, 1–15 hours for transit durations, 1–10 days for phase curves). Additionally, as much thermal ancillary data as possible should be gathered, with sufficient resolution and precision for use in post-processing.

Another source of noise in the *Kepler* flux time series is due to the pointing of the spacecraft. *Kepler* met its pre-launch requirement of 3 mas (~ 1 millipixel) pointing jitter in 15 minutes and had a measured month-to-month drift of 10–15 millipixels. In general this very precise pointing largely eliminated the requirement for absolute flat-fielding. Problems arose, however, when there were sudden offsets in the pointing, such as pointing adjustments (“tweaks”) to adjust the spacecraft attitude. These typically generated discontinuities in the flux time series that were substantially more difficult to detrend than slow drifts. In the early part of the mission, *Kepler* was forced to make several pointing tweaks, which significantly degraded the photometric precision of those data. The Attitude Determination Control System (ADCS) was modified to eliminate the drifts necessitating the tweaks. *Pointing changes during observations should be avoided to the greatest extent possible.*

Several electronic artifacts impact *Kepler* photometry, including undershoot (an apparent reduction in pixel sensitivity downstream of saturated pixels for up to 20 pixels), Moire pattern noise (due to a temperature- and time-dependent resonance in the Local

Detector Electronics (LDE) amplifier circuit aliased to near-Nyquist spatial frequency), rolling bands (due to the same resonance aliased to near-zero spatial frequency), and both FGS and electronic cross-talk. *Early detector calibration tests allowed identification and significant mitigation of the undershoot effect and demonstrated the power and indeed, the necessity, of robust, early detector characterisation.*

Finally, not only the temperature but the speed of the reaction wheels was found to impact *Kepler's* photometry. When any of the wheels were going through zero RPM, degraded pointing precision resulted in increased photometric noise. If there is the ability to manage the times at which the reaction wheels have zero crossings, care should be taken to avoid critical times of interest, e.g. transit ingress or egress. In addition, after the failure of the first reaction wheel, the remaining three wheels were routinely operated at significantly higher RPM than before, which resulted in improved pointing precision and decreased noise in the photometry. Of course, longevity of the reaction wheels should be considered in any decision about operating RPM, but this was a happy outcome of the increased RPM.

It is encouraging to note that initial reductions of K2 data are showing nearly the same level of precision as *Kepler's* primary dataset. The effects of modestly degraded pointing performance have been mitigated by standard decorrelation techniques.⁶

4.3. The Spitzer Space Telescope

Spitzer is a 0.85-m infrared telescope that was launched in 2003. On-board it hosted the Infrared Array Camera (IRAC; 3–8 μm), the Infrared Spectrograph (IRS, 5.3–40 μm), and the Multiband Imaging Photometer for *Spitzer* (MIPS; 24, 70 and 160 μm) instruments. In May, 2009 its supply of liquid helium was exhausted and the longest wavelengths were

⁶<http://keplerscience.arc.nasa.gov/K2/Performance.shtml>

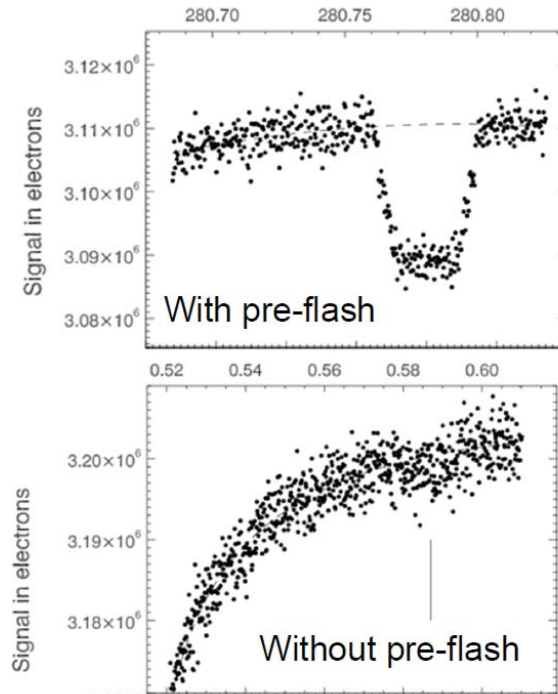


Fig. 9.— *An example of the ameliorating effect of pre-flashing the IRAC 8 μm detector is shown in the comparison between two observations of GJ436 (Seager & Deming 2009). The bottom panel shows the steep rise in signal without pre-flashing, the top panel shows the improved performance with flashing (Carey (2014), this workshop).*

no longer usable. However, in its Warm Mission phase *Spitzer* has continued to obtain high precision infrared photometry with the shortest two bands of the IRAC instrument.

4.3.1. IRAC

Despite numerous challenges, the IRAC instrument has been able to achieve a precision level of 25-30 ppm for transit measurements with both its In:Sb and Si:As detectors (Knutson et al. 2009; Fraine et al. 2013). The noise level continues to improve as the square root of the number of epochs for a non-variable host star (Demory et al. 2012)

so that stacking multiple transits is an effective technique to improve SNR. This section describes some of these challenges and the mitigation in either spacecraft operations or post processing needed to achieve these levels of precision.

One prominent systematic in the flux time series generated with IRAC is a substantial ramp in the photometry in the 8 μm channel. This was attributed to charge-trapping in the detector material, changing the effective gain in those pixels. The timescale for filling the traps in a given pixel depends on the flux falling on that pixel, ranging from 1–24 hours, with the amplitude of the ramp ranging from 1–10%. One strategy that was developed to mitigate this effect was by ‘pre-flashing’ the detector—observing a bright target and filling the charge traps before moving to the target of interest—and correcting the results on a pixel-by-pixel basis (Figure 9; Seager & Deming (2009)).

The same Si:As detector in the 5.8 μm channel exhibited the opposite behaviour—an anti-ramp that was possibly caused by a persistence effect in the read-out multiplexers. This effect occurs over a timescale of hours and is flux-dependent as it is not observed at low flux levels. The typical post-processing strategy was to use the data themselves to fit the ramp, with the caveat that the effect may be over-fit in this fashion.

As with *Kepler*, the spacecraft pointing is a significant source of correlated noise in the photometry. For *Spitzer*, the pointing variations consist of (1) semi-regular pointing wobble, with an amplitude of $\sim 0.08''$, and a period of 36–60 minutes, (2) pointing drift of $0.3''$ per day in 80% of observations, and pointing jitter of $\sim 0.03''$. The IRAC pixels are $1.2''$ in size and are thus undersampled, which increases the noise introduced to the photometry due to intra-pixel variations. The most successful strategy for removing these variations has been to build a high fidelity intra-pixel gain map for well-behaved pixels in the two remaining IRAC channels. The observations are then placed onto these pixels, and the gain map is used to detrend the data in post-processing (Figure 10a).

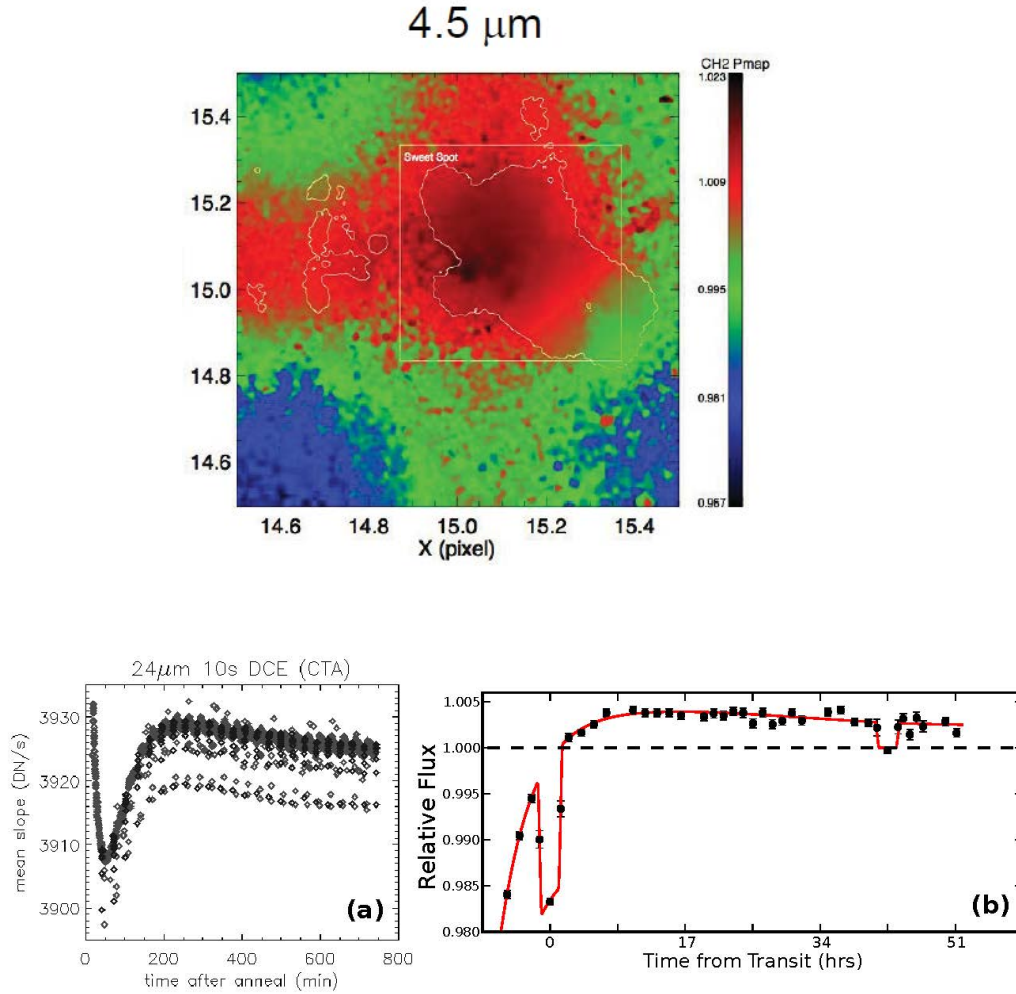


Fig. 10.— top) The pixel gain map used in *Spitzer* transit observations at $4.5 \mu\text{m}$. Many calibration observations were used to generate the map of the responsivity of this specific pixel. Transit targets were then placed accurately on the marked square known as the “sweet spot”. Bottom) Examples of detector systematics: MIPS $24 \mu\text{m}$ detector ramp and subsequent fallback as seen in pre-launch lab tests ((a); Young et al. 2003) and on orbit in observations of HD 209458b (panel (b); Crossfield et al. 2012). Without sufficient lab tests and documentation, the decrease in flux seen in (b) could be mistakenly interpreted as a planetary phase curve. (Carey (2014), this workshop).

4.3.2. *IRS & MIPS Photometry*

Spitzer's Si:As cameras, used for 16 and 24 μm photometry with IRS and MIPS (Rieke et al. 2004), provide yet another set of lessons for optimal, highly stable, photometry. These derive from the various instrumental effects: temporal variations in detector sensitivity, and nonuniform detector response coupled to variations in telescope pointing.

The MIPS 24 μm instrumental response varied across the field of view, even after calibration including flat-field corrections. In the MIPS instrument, every time series was obtained by dithering across 14 different dither positions. The sensitivity at each position varied by $\sim 2\%$, introducing unnecessary systematic offsets into the photometry. Fourteen positions is an excessive number, but this effect is not wholly undesirable – data acquired at multiple, independent positions can provide an internal consistency check. More serious was pointing-dependent sensitivity variations which varied at different dither positions, possibly attributable to flat-field errors (Crossfield et al. 2010). Because this effect did not correlate with pixel phase, residual flat-field errors seem a more likely source than intra-pixel variations; applying an empirical flat field generated from the data themselves may slightly reduce the impact of this effect (Crossfield et al. 2012). Unfortunately, the flat-fielding explanation means that pixel-mapping does not effectively mitigate the effect and so a large number of polynomial terms (one set per dither position) must be employed. The primary lessons from these effect are: (1) *do not dither across $\gtrsim 2$ positions*; (2) *minimize pointing variations during long time series*; (3) *pay closer attention to accurate and precise flat-field corrections*.

Several electronic effects were also observed in the MIPS data. These include a ramp in the flux time series at the start of some observations ($\sim 2\%$, lasting 2–10 hours), similar to that seen in IRAC 8 μm data (Crossfield et al. 2012). Unlike the IRAC ramp, the MIPS ramp occurred only occasionally (perhaps related to recent thermal anneals of the detector).

There is some evidence that even over 60 hr the instrumental response had not stabilized, instead transitioning from ramp to a $\sim 0.2\%$ “fall-back” in sensitivity after 10–30 hours (see Fig. 10; this effect was characterized rather poorly, to the extent that it precluded any definitive statement about HD 209458b’s thermal phase curve (Young et al. 2003; Crossfield et al. 2012). For transits and eclipses the ramp can be removed by simultaneous fitting of a transit light curve and ramp function. Many functional forms must be tested, and the final choice of function must be statistically justified (e.g., Stevenson et al. 2012). Failure to follow this approach can result in significantly underestimated uncertainties.

Bright and dark latents are also apparent in the MIPS observations, which can persist for days, and are a potential source of noise in photometry even when recognised. One suggested strategy is to take several frames at one position, then offset the telescope for the main science observations. This approach allows identification of latent regions and hot & bad pixels. *As was suggested for Kepler, pre-flight calibration tests for detailed detector characterisation are extremely useful in identifying the source and form of the signals for subsequent mitigation.*

5. *JWST* Operations for Transits

5.1. Observatory Overview

Although it was not optimized for transit operations, many aspects of the observatory will make *JWST* a superb platform for high precision observations. The instruments and detectors are described in §6 and §7. In this section we describe aspects of the observatory relevant to transit observations.

JWST’s optical quality is excellent with diffraction limited imaging at $2\ \mu\text{m}$. The wavefront error budget that determines the image quality comprises static and dynamic

allocations for the telescope topics, the ISIM and the science instruments, combined with pointing jitter. The imaging performance at wavelengths less than $2 \mu\text{m}$ is not diffraction-limited, but still provides excellent image quality for photometric and spectroscopic observations. Performance limitations imposed by the stellar image will arise from the sampling and the intra- and inter-pixel variations of the detectors within individual instruments.

While HST showed significant orbit-to-orbit changes in PSF due to thermal effects in low earth orbit, JWSTs highly stable L2 orbit should result in very low levels of wavefront drift. JWSTs requirement (worst case) is 57 nm over 14 days, after slewing from its hottest to its coldest pointing configuration. It is expected that more typical wavefront errors should be < 10 nm over a single observation compared with ~ 30 nm over an HST orbit (Gersch-Range & Perrin 2014). More significant changes might arise in phase curve observations lasting a few days. These effects will be studied early in the commissioning of JWST. Careful scheduling of transit measurements to avoid large slews before settling on a transit target might further mitigate the effects of thermal drifts (Gersch-Range & Perrin 2014).

Kepler and *Spitzer* demonstrated the critical importance of first minimizing position drifts relative to target pixels and second of having sufficient knowledge after the fact to enable decorrelation techniques to remove the effects of drifts on photometry or spectroscopy. The nominal *JWST* requirement on image motion is ~ 6.6 - 6.8 mas for the near-IR instruments and 7.4 mas for MIRI (per axis on any 15 second interval over a 10^4 second observation). For NIRC*am* this motion corresponds to an rms jitter of 0.1-0.2 pixel in the long or short wavelength cameras, or 0.05 - $0.1 \times$ the 2 pixel height of the NIRC*am* grism. For NIRSpec with its poorly sampled PSF (the core size is ~ 1 detector pixel) the jitter effects will be worse whereas for NIRISS with its ~ 20 pixel high spectra drift effects

should be greatly reduced. Finally, for MIRI with its 110 mas pixels, the relative jitter will be small, 0.06 pixel, although responsivity variations in the less well behaved Si:As detectors may amplify the jitter effects at longer wavelengths (§4.3.2). After the fact decorrelation using accurate position determinations can greatly reduce the effects of jitter as has been demonstrated with *Kepler* and *Spitzer*.

Spitzer's pixel-mapping technique (Figure 10a) proved to be very powerful in improving photometric precision. On *JWST* it will be possible to use the Fast Steering Mirror (FSM) to map out intra-pixel variations within “sweet spots” on the detectors. For *JWST*, FSM offsets with a precision of few mas will allow an image to be stepped around individual pixels to map out pixel response functions.

A technique recently demonstrated on HST of scanning the stellar image across a large number of pixels is being considered for *JWST*. Fast, large scale motions across many pixels could improve the saturation limit and reduce flat-fielding errors by averaging over many pixels, but flight software and new operational modes would have to be developed to support this technique. The use of moving target capability would provide spatial scanning but at much slower rates up to ~ 60 mas/sec.

The requirement for long, uninterrupted transit observations under extremely stable conditions over 6-12 hours (and even up to a few days for phase curve measurements) presents a variety of challenges. Some challenges have already been identified and resolved, some have been identified and should be solvable with appropriate attention paid to them, some will require significant resources and a high level commitment to resolve, and finally some may be so fundamental to the operation of the observatory or the instruments that they may never be resolved, only mitigated.

The four basic limits to long, uninterrupted observations include the following:

- *Re-pointing of the High Gain Antenna* nominally occurs every ~ 10000 sec. Even though the observatory remains in fine-lock, an HGA re-pointing will cause small (< 70 mas, or 1-2 NIRCcam pixels!), short (< 1 min) pointing disturbances. The project is working to provide the option of deferring re-pointings around transit observations or, at a minimum, to allow transit observations to observe through a re-pointing without forcing a break in the instrument cadence. Either approach is, at least, preferable to stopping and restarting exposures which would likely result in data gaps and/or response drifts.
- *Momentum wheel unloads* are planned to occur every 25 days, but could occur as frequently as every 5 days. While this is unlikely to represent a significant problem for most observations, STScI will have to investigate balancing the scheduling of transit observations to avoid interruptions with the competing need to minimize the buildup of momentum and thus minimize the consumption of propellant, a limited resource.
- *Station-Keeping maneuvers* occur every 20 days to maintain the orbit around L2. This is unlikely to be an issue for the majority of transit observations.
- *Wavefront Sensing* to maintain image quality is planned to occur every 2 days with the possibility of shifting an event by ± 1 day. In principle, it should be possible to schedule these activities to avoid transit observations. In practice this will depend upon wavefront error stability observing in orbit over the 14 day WFSC cadence.
- Maximum exposure duration is limited at the detector and/or instrument level, as described in Sections 5.2.1 and 7.

5.2. Observatory Operations for Transit Science

5.2.1. Exposures Overview

Exposures are executed in a completely regular, structured manner. Frame times, reset patterns, and the intervals between them are deterministic and invariant during an exposure. Clocking, reading and resetting of the detector pixels occurs at a constant cadence throughout the exposure. There are no irregularities in the cadence: data flows through the ASIC to the spacecraft without interruption. There is no difference, from the perspective of the detectors, between frames that are stored and frames that are discarded: the ASIC amplifies, digitizes, and packetizes *all* frames, and then simply marks the data appropriately afterwards. This exceptionally regular mode of running the detectors should result in exceptional photometric stability, particularly within exposures and after any (possible) transients that may occur at the beginning of exposures.

Details of frame times in full-frame and subarray modes for both H2RG and MIRI detectors are provided in Appendix B.

For the 3 instruments using H2RG detectors (NIRCam, NIRISS and NIRSpec), the maximum number of integrations within a single exposure, NINT, is 65535. For bright host stars, where short integrations will be needed in order to avoid saturating the detectors, this limit may result in transits to be observed using multiple *exposures*. In other words, after 65535 short integrations have been collected in the manner described above, the detector would return to idle mode, the end of that exposure would be detected by the scripts, and a new exposure command would be issued. The effect of such exposure breaks on photometry, at the precision relevant for transit science, is unknown and exceptionally hard to determine on the ground. Unfortunately the NINT limit is inherent to the design of the ASIC and can not be circumvented. Table 2 gives maximum exposure durations for

a few relevant subarray configurations.

5.2.2. *Data Volume and Data Rates*

All science and engineering data produced by *JWST* and intended for downlink is temporarily stored on the solid state recorder (SSR). One half of the SSR capacity is available daily, the other half retaining a copy of older data as insurance against potential downlink failures. For science data, the available daily data volume is 57.5 GB. Transit observations, with their high photon-collection duty cycle, integrations that will typically use $NFRAMES = 1$ (i.e. no coadding, and very lengthy observations, could significantly strain the data volume allocation.

The data rate from the H2RG detectors depends on whether the detector is configured in full-array (or subarray stripe) mode, or in subarray mode. As mentioned earlier, in normal subarray mode the all the pixels are read out through a single output channel; the data rate in this mode (neglecting small overheads for telemetry values) is approximately 16 bits every $10 \mu\text{sec}$, or 1.6 Mb/sec. Running continuously for a day, this equates to 17.3 GB/day. In full-array and stripe modes the pixels are read out through 4 output channels in parallel (each output handling pixels in a 512-column wide region), and the data rate is 4 times larger: 6.4 Mb/sec or 69.2 GB/day. These data rates neglect the fact that no data is generated during reset frames – for short integration ramps the resets can reduce the data rate by as much as 50% (for $NGROUPS=1$, $NFRAMES=1$). However, comparing these *single-detector* data rates to the SSR allocation given above, it becomes clear that there is the potential for transit observations to overfill the SSR. This is particularly true for NIRC*am* because of the large number of detectors. To avoid exceeding the daily SSR allocation NIRC*am* data will only be taken using two detectors (one each in the short-wave and long-wave channels). NIRS*pec* transit observations will use a single output (window

Table 2. Maximum Exposure Duration, H2RG Detectors^a

Subarray Configuration	Frame Time (sec)	Integration Duration (sec)	Exposure Duration (hr) ^b
64×64^c	0.0494	0.148	2.7
160×160^c	0.277	0.831	15.1
2048×64^c	1.34	4.02	73.1
2048×64^d	0.341	1.02	18.6
2048×2048^e	10.74	32.2	586

^aFor integrations with two NFRAMES=1 groups.

^bEach exposure is limited to a maximum of 65,535 integrations.

^cNormal subarray, using a single output channel.

^dStripe-mode subarray, using 4 parallel output channels.

^eFull-frame mode, using 4 parallel output channels.

mode) and should not present data rate problems. Other minor restrictions in the observing templates for transits will guarantee that the data volume limit is not violated.

5.2.3. *Event Driven Operations*

JWST will use an event-driven observation schedule, rather than one where observations are all initiated at a pre-planned absolute time. The event-driven approach should provide higher observatory efficiency because any failed observations can (usually) be immediately followed by the next observation in the queue. The event-driven observation plan *is* a strict queue: observations will execute in the order specified in the observation plan. Observations consist of one or more visits to a target or pointing. Observations may have to be composed of multiple visits, for example, if more than one guide-star is required in order to complete the observation. Photometry of a point source, including small dithers, could be accomplished using a single visit. Mapping of a region or an extended source, where offsets larger than about 20'' are required, would be executed as multiple visits. Exoplanet transit/eclipse observations will be executed as single visits.

While most observations will begin when event-driven operations allow them to be, *observers are allowed to specify fixed-time constraints*. Observatory requirements dictate that such observations will begin within ± 2.5 minutes of the observer-specified start time. Some additional flexibility will be available for planning and scheduling recurring events such as transits and eclipses. Observers will be able to specify a desired PHASE for the start of their observation, providing schedulers with multiple opportunities to include their observation into the observing plan. Once the schedulers put the observation into a plan, the PHASE constraint will be converted into the fixed-time constraint appropriate to the planning period.

When the observation plan includes a fixed-time observation (such as a transit or eclipse), schedulers will estimate the time required to execute all prior observations in the plan and include enough margin such that the observatory will be prepared to begin observing at the appointed moment. If a prior observation fails, the observatory will remain idle until the next observation (whether it is unconstrained or has a fixed-time constraint) can begin. All observations have validity windows during which they can begin. These windows, for all targets, depend on guide-star availability and any other observer-specified constraints. Guide stars must be usable for the entire duration of a visit to a target. The observation plan includes multiple guide stars for every target or pointing, and includes the visibility windows for each guide star. The guide star is chosen from that list by the on-board scripts at the time the observation is actually ready to start.

The event-driven operations planning system for JWST is designed from the outset to take into account the possibility that individual observations may fail. Current modeling of the scheduling process indicates that this possibility can be accommodated by including several observations with execution windows that open at (or soon after) the transit observation timing constraint. The schedule can then adjust to the failure of even quite long observations. The active observation plan **would** end earlier than previously predicted in such a case, but there would be adequate time to react to the failure and append to the observation plan to avoid any periods in which the observatory became idle.

5.2.4. *Observation Planning*

Observation planning for *JWST* will make use of the Astronomers Proposal Tool (APT), familiar to many who have observed with *HST*. Transit observations will have their own user interface because of the unique requirements they will place on the observatory, and to provide a clean, intuitive interface for science users. As mentioned above, the

PHASE constraint will allow observers to specify that they want an observation starting at a particular orbital phase for a transiting planet without having to specify exactly which transit event they wish to observe.

Saturation will be a significant issue that must be addressed during observation planning for transit science. Details regarding the saturation limits for the various instruments are summarized in Section 7, and can be used with a reasonable degree of confidence now. By late 2016 APT will include direct access to an exposure time calculator (ETC). The ETC will provide saturation estimates for sources, and APT will issue warnings if an observer specifies exposure parameters that would result in saturated science images.

Another key aspect of transit observations will be balancing requirements for avoiding saturation of the detectors (accomplished through choice of subarray size and number of groups and frames in each integration ramp) with the need to take very long exposures. For bright stars it may be impossible to do both without breaking the observation into multiple exposures, as discussed earlier. Given a target star or flux estimate, the proposal tool will provide information on saturation limits in the various available modes (see Section 7), and suggest possible exposure parameters. Once the user picks an observing mode and set of exposure parameters, the system will indicate the total exposure duration and allow the user to select multiple exposures if that is required in order to get a time-series spanning the event and out-of-event baselines. The exposures, if more than one is necessary, would be executed with the minimum possible gaps, and with no interruptions for other engineering or science activities.

The current plan is to include a target acquisition (TA) step as an integral part of the transits observing template. For the slitless grism modes of NIRISS and NIRCам, TA is required in order to know the wavelength calibration of the data. For NIRSpec, TA is required to accurately place the target into the dedicated slit, thereby minimizing

slit losses and pointing-dependent photometric variations. The need for TA in NIRCcam imaging modes is less clear given that the NIRCcam pixels sample the PSF rather well, and intrapixel sensitivity variations for the H2RG detectors appear to be quite small. (This is unlike the situation with, e.g., Spitzer/IRAC, where pixel variations are a significant effect that is magnified by the under-sampling of the PSF.) Nevertheless, by repeatedly observing transits on the same real-estate on the NIRCcam detectors, it may be possible to derive extremely precise methods of calibration of the data.

5.2.5. *Transit Timing*

The timestamp for transit events is important for easy inter-comparison of transits from multiple observatories to look for small timing transit variations (TTVs) due to planet-planet interactions. The community has identified *BJD_TDB*, which uses the barycenter of the solar system as its reference point. *TDB* is a barycentric dynamical time and it is distinct from *UTC* in that it doesn't have leap seconds (Eastman et al. 2010). Spitzer adopted the approach of providing timing information in a variety of ways. Table 3 gives an extract from a Spitzer FITS header.

The precision needed for absolute timing is driven by TTVs requirements. The uncertainties in the measured midpoint of a well sampled, relatively high SNR transit measured with *Kepler* can be as low as a few seconds, particularly with short cadence data. Thus, to avoid increasing the uncertainties in a TTV measurement, the after-the-fact, absolute timing uncertainty in *JWST* measurements should be $\ll 1$ minute. These issues are under active study by the *JWST* project.

6. Detector Issues and Features

6.1. HgCdTe Detectors for NIRCam, NIRISS and NIRSpec

Three of *JWST*'s instruments share a common detector technology, using 2048×2048 pixel, *H2RG* detectors from Teledyne Imaging Systems with either short- or long-wavelength cutoff material. For many of *JWST*'s programs the critical parameters will be high quantum efficiency (QE) and low read noise, and the newly installed devices in NIRCam exceed project requirements with an average QE of 0.90 ± 0.05 at $2 \mu\text{m}$ and 0.85 at $3.5 \mu\text{m}$. Total noise in a 1000 sec observation from read noise and dark current is $6 e^-$ in the short wavelength arrays and $8 e^-$ in the long wavelength arrays. But for transit observations which stare for long periods of time at bright sources, a different set of parameters become important, including long term stability, inter- and intra-pixel variation of QE, persistence, readout speed and well-depth before the onset of non-linear effects. As described in the discussion of the individual instruments (§7), the subarray capability of the H2RGs allows *JWST* to observe very bright sources, particularly when combined with a high spectral resolution setting.

NIRCam tests have revealed latent images, i.e. persistent charge that bleeds off slowly after a bright sources is removed from the array. The persistence has the level of a few $e^- s^{-1}$ after illumination at 80% of full well and shows at least two times constants, ~ 60 and ~ 1000 seconds. A converse effect is slowly increasing responsivity at the start of an observation of a bright source may affect the first few hundred seconds of an *JWST* observation at the few 10s of ppm level.

Overall, the performance of *JWST*'s H2RGs should be excellent in the transit application with photometric precision of ≤ 25 ppm. This conclusion is based on laboratory tests (§6.4) and, most importantly, on existing space observations. *HST*/WFC3 uses a

1.7 μm cutoff H2RG and has achieved 70 ppm precision per band-integrated exposure and a final precision on spectroscopic transit depths of 25 ppm for 5-pixel-wide binning. (Kreidberg et al. 2014).

6.2. MIRI Detectors

The detector arrays used in MIRI are the direct descendants of the long wavelength Si:As arrays used on *Spitzer*/IRAC. They have the same four science outputs, channel interleaving and readout procession, and overall noise performance. The chief differences are the larger format, 1024×1024 vs 256×256 , and a slightly smaller pixel size, 25 μm vs. 30 μm . As discussed in §7.4, the detectors can be operated in a variety of subarray modes which will enable observations of bright sources for transits.

Just as with IRAC (§4.3.1), there are numerous detector pathologies that will have to be mitigated against in observation planning and in post-processing. Some of the bad habits affecting transit observations are listed below:

- Response drifts during exposure – a serious problem for transit observations as identified in *Spitzer* observations (§4.3.1).
- The Reset anomaly represents “left-over” signal from previous resets which contaminate the beginning of subsequent integrations. Fortunately, the effect is not flux dependent and can be corrected with information extracted from darks.
- Latent images on timescales from a few seconds to a few hours. The largest component has an 8 sec time constant, a 2 min time constant term has an $800 \times$ smaller amplitude, and there is a 10 min effect with even smaller amplitude ($1 \times - 4 \times$). The effect manifests itself as latent images in subsequent exposures.

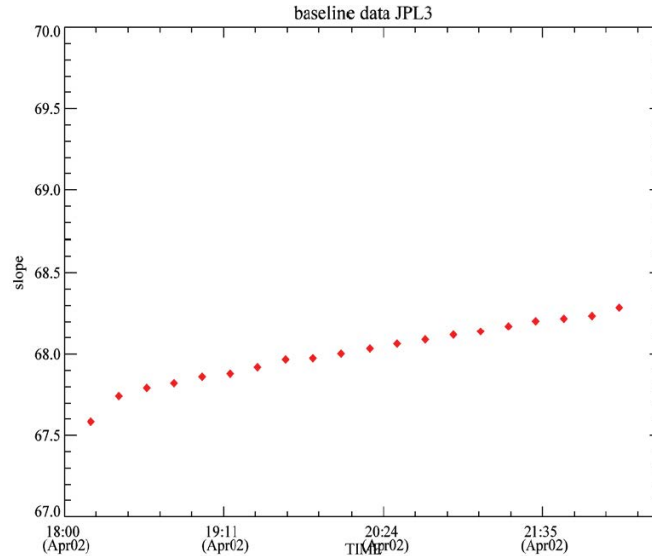


Fig. 11.— A long 4 hour exposure shows a long term drift of $\sim 1\%$ in the responsivity of a MIRI Si:As detector under constant illumination. (Ressler (2014), this workshop).

- Settling when changing operational mode. Switching in or out of subarray mode can unsettle the detectors for up to 20 minutes and observations should be planned to avoid unnecessary switching.

Figure 11 shows an example of a $\sim 1\%$ change in response over a four hour exposure. Effects like this are seen in IRAC and will have to be corrected for in post-processing. Figure 10 shows similar effects in *Spitzer*/MIPS detectors.

Overall, however, the MIRI detectors are very sensitive and very good cosmetically. Extensive calibration efforts are ongoing and will continue throughout flight operations. *Spitzer*/IRAC experience should be an excellent guide to planning for *JWST* /MIRI observations.

6.3. Efficient Detector Readout Scenarios and Bright Star Limits

Most of the *JWST* detectors have a readout arrangement optimized for lowest possible noise for long integrations. Such arrangements can be inefficient for the short observations of bright sources required for transit measurements. The region of interest must be readout three times in a frame-wise “*RESET – READ – READ*” pattern with each step requiring a read time, T_r : 1) reset, 2) read frame (initial value) and 3) read frame (final value). The measured signal then equals the final read (#3) minus the initial read (#2). Although the total exposure time is $3 \times T_r$, the time over which useful photons are collected is only T_r for a duty cycle of 33%. As much signal accumulates prior to the first read as during the actual integration so bright limit is halved. Furthermore, more photons accumulate

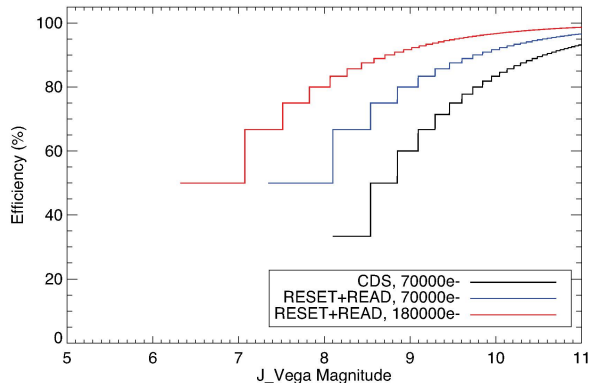


Fig. 12.— *NIRISS* On-sky efficiency during integration as a function of target *J*-band magnitude for 3 read-out schemes, the standard correlated double sampling (*CDS*) mode, the reset+read mode and a boosted detector gain mode. This is for the Standard mode with a sub-array size of 256×2048 pixels. The curve ends at the onset of saturation. The curves would shift to the left by 1.2 magnitudes when observing with the Bright mode (80×2048 pixels). The pixel-wise “*READ – RESET – READ*” would approach 100% efficiency up to a saturation limit set by the frame readout time.

after the final read, resulting in more charge trapping and image persistence. A variant of the frame-wise (*RESET – READ – READ*) pattern uses only a (*RESET – READ*) to improve efficiency to 50% and reduce overall charge accumulation (Figure 12). The penalty of this variation is uncorrected *kTC* noise $\sim 35e^-$, which would, however, be small compared to the stellar shot noise for bright sources, $\sim 245e^-$ at 80% of full well. A larger concern for the *RESET – READ* mode is the long term stability of the per-pixel DC offset which is no an issue with *RESET – READ – READ*.

An alternative approach for improved efficiency uses a per pixel-“*READ – RESET – READ*” pattern: 1) address a pixel, 2) read final value of previous exposure, 3) reset that pixel, 4) read initial value for next exposure and 5) move to next pixel. The advantages of this approach is near 100% duty cycle and a reduction in the charge on a pixel past the final read so persistence effects will be reduced.

Finally, a hardware approach to improving the saturation limit and overall efficiency would increase the bias voltage on the HgCdTe detectors to increase the well depth to $\sim 180,000 e^-$. This change would yield a ~ 1 mag improvement in limiting magnitude and an increased efficiency (Figure 12), but is as yet untested in terms of noise performance or an increase in the number of hot pixels and other detector artifacts.

Incorporating new readout schemes into the flight software for the instruments will require significant effort including testing to ensure that subtle side-effects do not otherwise degrade the performance of the detector. It is not yet clear that the scientific return is sufficiently compelling to warrant such changes.

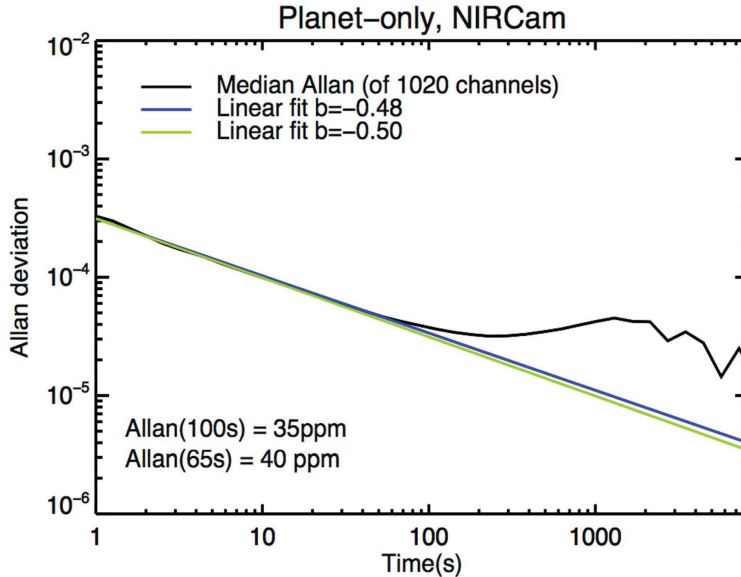


Fig. 13.— An Allan Deviation plot showing shot noise limited performance of a NIRCAM-like simulated spectrum at a level of 35 ppm before leveling off. (Beichman (2014), this workshop)

6.4. Laboratory Tests of HgCdTe detectors for Transit Observations

A laboratory testbed has been established at Caltech with the express purpose of testing HgCdTe detectors in transit applications. Initial experiments were aimed at demonstrating levels of precision suitable for an infrared all-sky transit survey (Clanton et al. 2012) using a $1.7 \mu\text{m}$ H2RG detector similar to that used on *HST*/WFC3. With suitable decorrelation of pointing and lamp drifts it was possible to achieve a precision level for point sources of < 50 ppm. The testbed has been modified to project images of simulated spectra using monochromatic light. The simulated spectra have an extent in the dispersion direction of 1020 pixels and 1, 2 or 10 pixels in the spatial direction. These sizes are similar to the spectra produced by NIRSpec, NIRCAM’s grism, and NIRISS, respectively (although

the NIRISS has an extent of 20 pixels not 10, (§7.2). Figure 13 is an Allan Deviation plot for a NIRCams-like spectrum and shows that after decorrelation for lamp drifts and pointing drifts up to 0.5 pixels, the data average down as $t^{-1/2}$ as expected for photon-noise limited observations until reaching a floor of <35 ppm. In at least one experiment, observations with a simulated NIRISS spectrum achieved a noise floor of 20 ppm. Work with the Caltech testbed is continuing and will eventually use a flight-spare, short wavelength H2RG for higher fidelity testing. The NIRISS team is developing its own testbed capable of projecting a true polychromatic spectrum using a flight-like instrument configuration. These testbeds will be valuable for assessing the limits of *JWST* measurements, developing on-orbit procedures, and optimizing post-processing algorithms.

7. Instrument Modes for Transits

Transit observations require *JWST* instruments to operate in conditions rather different from those that have driven their design (with the exception of NIRISS). In order to detect light variations of the order of a few 10s of ppm over time scales of several hours, an accurate control of systematic effects such as intra-pixel sensitivity variations, linearity and image persistence becomes critical. The summary of instrument capabilities presented in this section will therefore focus on the characteristics most relevant for this type of observations. Further information, including a *JWST* Exposure Time Calculator, can be found at <http://www.stsci.edu/jwst/instruments>.

Figure 14 lays out the relevant modes of the four *JWST* instruments which will be discussed in the following sections. Figure 15 shows the same information in a different form, plotting spectral resolution as a function of wavelength. The saturation levels for different modes are given in Table 4 and shown graphically in Figure 16.

7.1. NIRSpec

NIRSpec is a near-infrared spectrograph capable of low- ($R \sim 100$), medium- ($R \sim 1000$) and high- ($R \sim 2700$) resolution spectroscopy between 0.6 and 5.3 μm (Ferruit et al. 2012). The combination of wavelength coverage and spectral resolution provided by the instrument will make it possible to resolve spectral features of many molecules expected to be found in exoplanet atmospheres, including H_2O , CO_2 , CO , CH_4 , and NH_3 . Although current space-based facilities can deliver spectroscopy of H_2O features (*HST*/WFC3) and photometry sensitive to CO , CO_2 , and H_2O (*Spitzer* 3.6- and 4.5- μm channels),

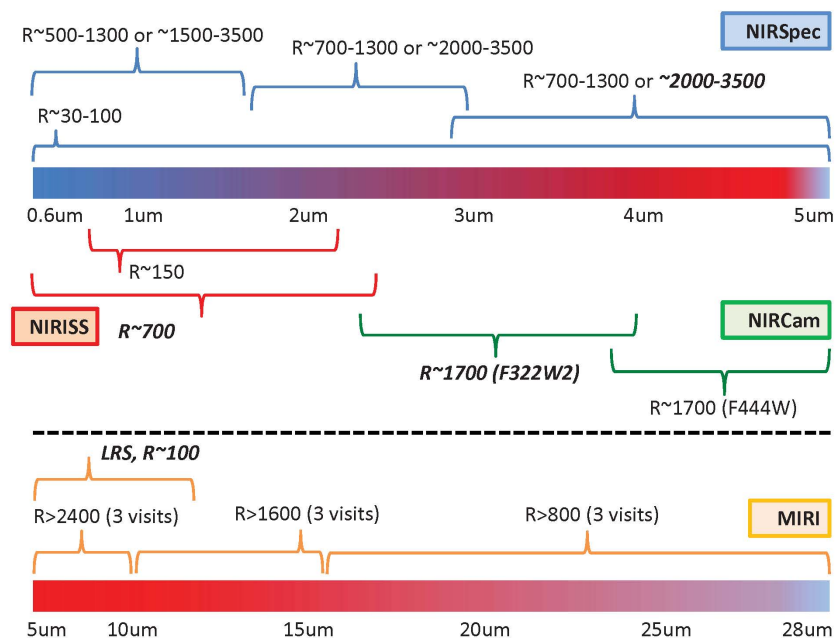


Fig. 14.— *As described in subsequent sections, a wide variety of instrument modes can be used for transit observations. In general, observations of at least 4 separate transits will be required for complete spectral coverage from ~ 1 to $>10 \mu\text{m}$. In some cases, for fainter sources $J < 11 \text{ mag}$ and at low spectral resolution, the NIRSpec prism mode can cover the entire 1-5 μm range.*

NIRSpec will provide improved resolution, sensitivity, and wavelength coverage, enabling new constraints on the elemental abundances of exoplanet atmospheres and their thermal structures.

The instrument can be operated in three different modes: multi-object spectroscopy (MOS mode) over an area of 9 square arcminutes with micro-shutter arrays for the selection of the sources; integral field spectroscopy (IFU mode) over a field of view of $3'' \times 3''$ and with a sampling of $0.1''$; slit spectroscopy (SLIT mode) using five high-contrast slits. *One of these five slits is a square $1.6'' \times 1.6''$ aperture designed specifically for exoplanet transit spectroscopy and it will be the primary mode for observing exoplanets with NIRSpec.*

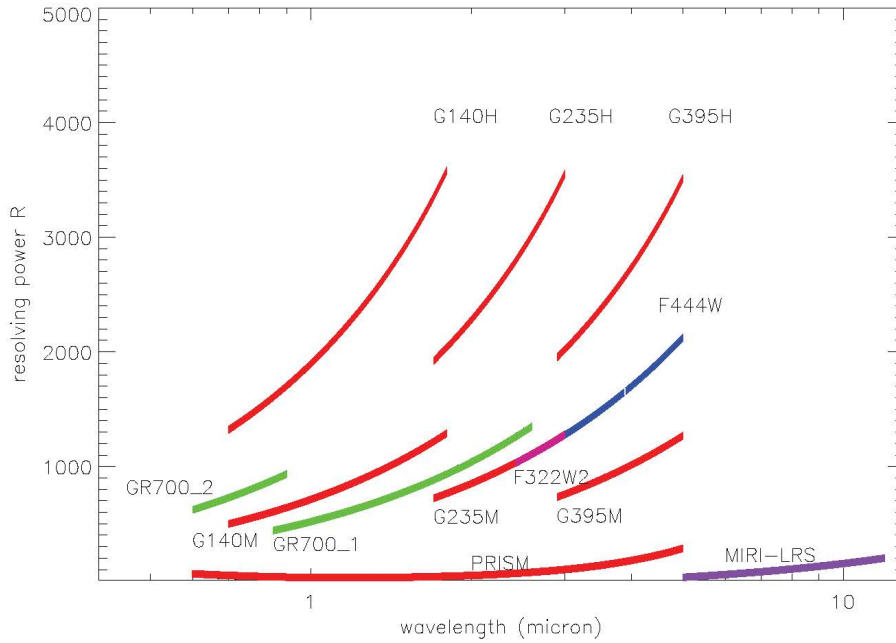


Fig. 15.— *The resolving power vs. wavelength is shown for all instrument modes relevant to transits. The instruments are coded by color: red=NIRSPEC; green=NIRISS; BLUE=NIRCAM; PURPLE=MIRI. There is an overlap between NIRSPEC-G235M and NIRCAM-F322W2, indicated with a violet area. The thin white line in the NIRCAM blue field separates F322W2 from F444W.*

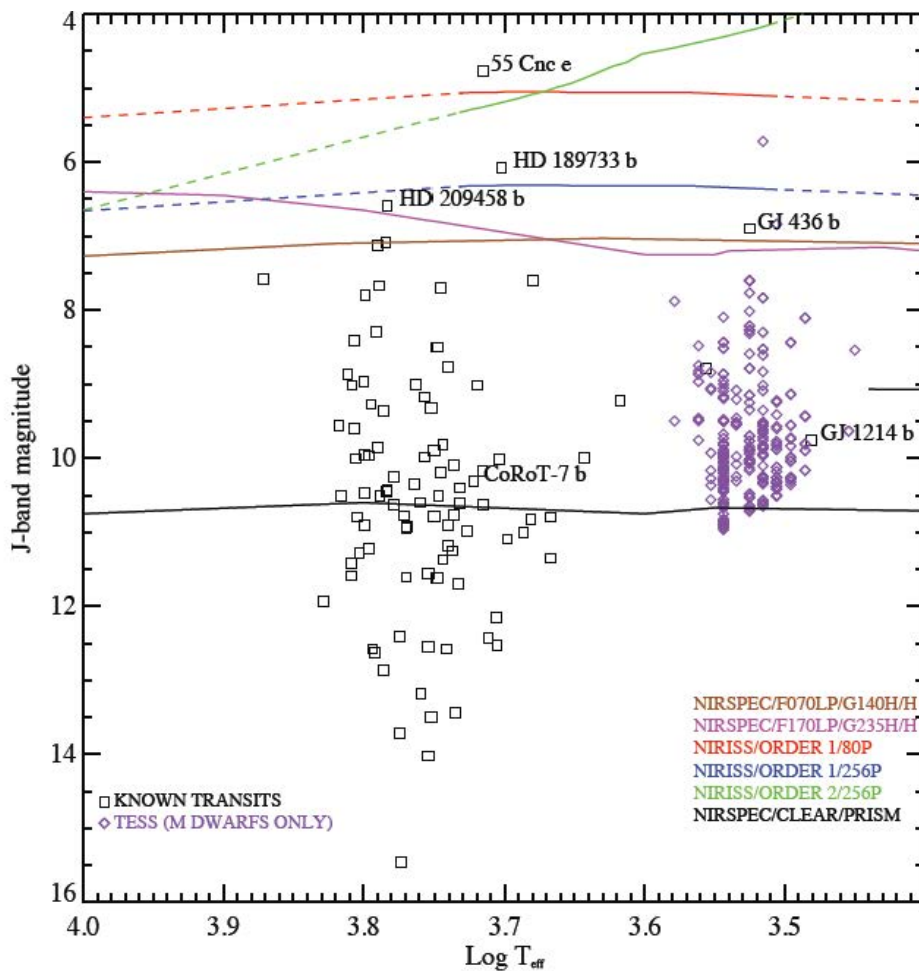


Fig. 16.— *The figure shows the saturation limits for various NIRSpec and NIRISS modes relative to the brightness of known transiting planet host stars. Stars below the lines can be safely observed in a particular mode. Note in particular the limit around $J=11$ mag for the prism. With its fast readout mode the NIRCcam grism can obtain spectra for sources as bright as $K\sim 3$ mag. (adapted from Ferruit and Birkmann (2014), this workshop).*

A summary of the characteristics of the spectral configurations of NIRSpec available for transit spectroscopy is provided in Table 5 with a plot of the associated spectral resolution curves found in Figure 14.

For science cases that do not require high spectral resolution, the low spectral

resolution mode of NIRSpec (CLEAR/PRISM, Table 5) provides very broad spectral coverage from 0.6 to 5.3 μm in a single exposure. This configuration has no equivalent in the other *JWST* near-infrared instruments. It also provides some wavelength overlap with the MIRI LRS configuration, opening the possibility to “stitch” NIRSpec and MIRI spectra together. Besides the low spectral resolution, the main limitation of this configuration is its relatively high saturation limit of $J < 11$ mag (Table 4 as well as <http://www.cosmos.esa.int/web/jwst/exoplanets>). For reference, the typical host star for the *TESS* planet detections is expected to have a K-band brightness < 10 mag (Dressing et al., in prep). This corresponds to J-band magnitudes of $< 10.5 - 11.0$ using a typical M-dwarf $J-K_S$ color index of 0.5 to 1.0 (Kirkpatrick et al. 1999). The saturation limit is worse at short wavelengths due to the combination of the typical stellar spectrum and the lower resolution of the prism at shorter wavelengths. This brightness limit becomes much less stringent for higher spectral resolution configurations. The worst case saturation limits correspond to J-band magnitudes of 8.5 and 7.5 for the medium and high spectral resolution cases, respectively (see <http://www.cosmos.esa.int/web/jwst/exoplanets> for more details).

The excellent sensitivity of NIRSpec means that the so-called “noise-floor” corresponding to an ideal observation limited only by the detector and shot noises will be low. As an example (Figure 17), only one hour of transit observation is necessary to reach a noise floor of 200 parts per million (ppm) for a 9^{th} magnitude host star (J-band). This means that NIRSpec transit spectroscopy programs will routinely have photon-noise limited noise floors of a few tens of ppm. It is therefore extremely important to be able to eliminate or calibrate out sources of systematic noise that could prevent us from approaching this theoretical limit.

There are several sources of systematic noise that may impact NIRSpec observations of transiting planets. We have listed the major ones in Table 6. It can be seen that the

raw contribution of one of these, intra-pixel sensitivity variations, is large compared to the targeted noise floor and will need to be removed with careful calibration. The good news

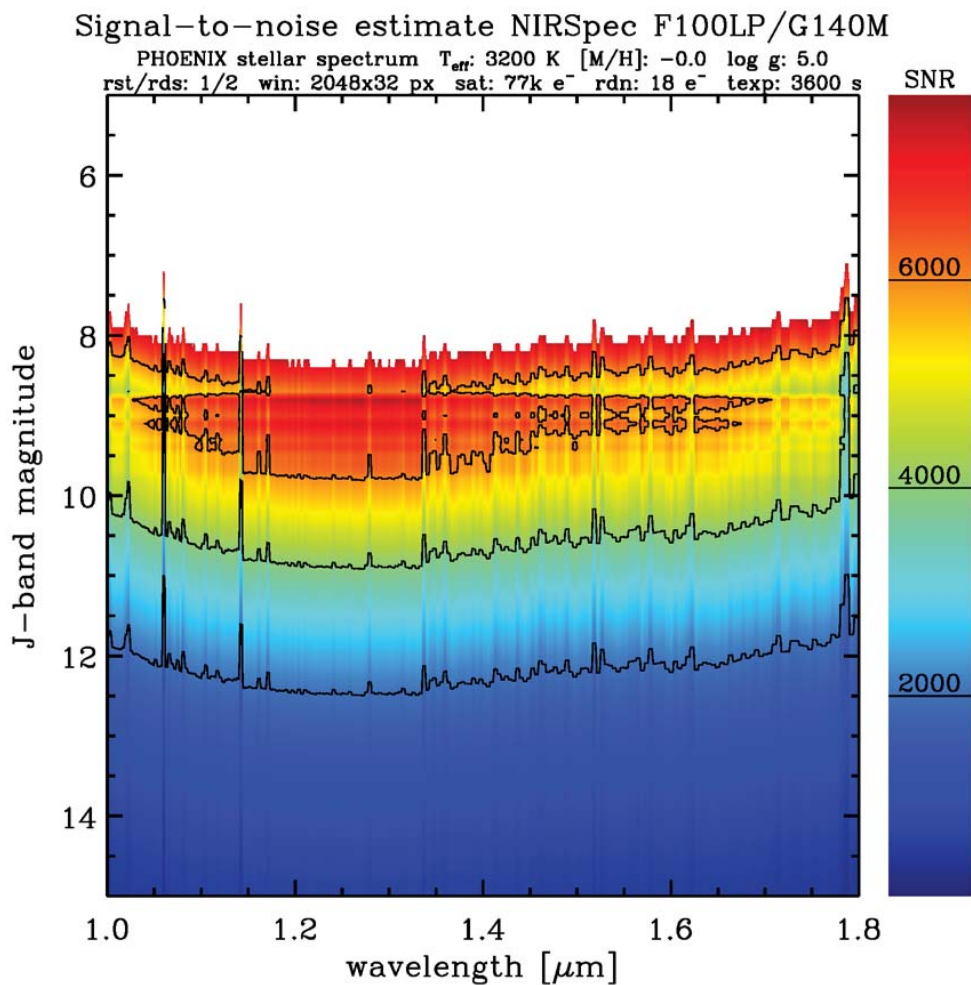


Fig. 17.— A plot showing the signal-to-noise ratio (detector and shot noise; no systematics) per spectral pixel for a transit spectroscopy observation at medium spectral resolution with NIRSpec (F100LP/G140M configuration) as a function of wavelength and of the host star J-band magnitude. The computation has been performed for a star with an effective temperature of 3200 K (M3–M4 typically) and an observation duration of 1 hour only. (Ferruit and Birkmann (2014), this workshop).

is that these systematics are similar to those affecting observations with *HST* and *Spitzer*, so that the analysis techniques honed for current data will provide a good running start for approaching the noise floor for NIRSpec observations. In many cases the sources of systematic error are expected to be reduced relative to earlier observatories, e.g. a more stable orbit relative to *HST* resulting in smaller focus drift drifts and greatly improved detector performance relative to *Spitzer* (§6.4).

Finally, there is a instrumental limitation on the duration of an uninterrupted transit or phase curve exposure with NIRSpec. A counter in the instrument hardware limits the number of integrations (*RESET – READ – RESET*) to a maximum of 65535. For the shortest integration time and baseline window size, this limits a single exposure to 12.5 hours (for the prisms) and 49.2 hr (for the gratings).

7.2. NIRISS

7.2.1. Instrument Overview

The Near Infrared Imager and Slitless Spectrograph (NIRISS) is the Canadian built instrument on the back plane of the Fine Guidance Sensor (FGS). Two filter wheels at the pupil plane accomodate three grisms (the GR150C and its orthogonal twin GR150R, and the GR700XD); a subset of NIRCcam filters (F090, F115, F140, F150, F158, F200, F277) a Non Redundant Mask (NRM) and its associated filters (F380, F430 and F480). Four operating modes are possible. 1) The Aperture Masking Interferometry (AMI) mode uses the NRM mask (seven holes spanning 21 interferometric baselines) combined with the red filters (F277 and redder) to search for companions at very close separation. 2) The Wide Field Slitless Spectroscopy (WFSS) mode uses the GR150 grisms. When coupled with one of the blue filters (F200 and bluer), they diffract in orthogonal directions and are destined

to study high- z galaxies. They could also be used, for example, for brown dwarf searches in young star clusters. They are not foreseen to be used for transit spectroscopy because of their very low resolving power ($R=150$), their faint saturation magnitude limit (~ 12) and the narrow spectral width spanned by the filter required to block higher orders. 3) The NIRCcam filter subset can in principle be used for direct imaging either as a NIRCcam spare or in parallel observing (not yet supported). 4) The last operating mode of NIRISS was specifically designed for transit spectroscopy. Its description follows.

7.2.2. Suggested modes for transit work

The Single Object Slitless Spectroscopy (SOSS) mode uses the GR700XD optics element — a crossed-dispersed grism whose first surface is a weak cylindrical lens to project defocussed traces in orders 1 and 2, insuring a simultaneous spectral coverage between 0.6 and 2.8 microns at a resolving power of about 700. The trace width is about 20 pixels in the spatial direction and Nyquist-limited along the spectral direction with the goals of minimizing flat fielding uncertainties and allowing bright targets to be observed without saturating.

7.2.3. Bright Star Limit

Two readout modes are currently implemented: 1) the standard readout mode reads 256x2048 pixels; 2) the bright readout mode reads 80x2048 pixels centered on the Order-1 trace between 1.1 and 2.8 microns (see figure 12). Both modes use a 1-amplifier read out with a duty cycle/read time of 16.47 (5.49) seconds and 5.66 (1.89) seconds, respectively. The bright readout mode exists specifically to improve the saturation limit and observe brighter stars. Figure 19 is a cut through the PSF along the cross-dispersed direction to

show how light is spread over the ~ 20 pixel-wide trace. Upon saturation, it is the pixels in each peak that saturate first while pixels in the core of the trace can tolerate ~ 0.7 magnitudes of further abuse. The peak efficiency of the grism is between 1.0 and 1.5 microns in Order-1 and between 0.6 and 0.8 microns in Order-2 so that is the wavelength range where saturation occurs first. Order-2 has twice the spectral dispersion of Order-1 and also has worse throughput which means that the Order-2 trace can tolerate an additional ≈ 1.0 magnitude before saturating. Assuming that saturation occurs at a detector count 70 000 electrons/pixel, using the beginning of integration throughput curves, then the saturation limit for correlated Double Sampling (CDS - *RESET* – *READ* – *READ*) images is at $J_{Vega} = 8.1$ in standard read out and $J_{Vega} = 6.9$ in bright read out. Approaches to improving these limits are discussed in § 6.3

7.2.4. Target Acquisition and Pointing Requirements

Target acquisition for the SOSS will consist in slewing to the target, configuring the dual wheels in the NRM+F480 filter (allows acquiring targets as bright as magnitude 3 without saturating) and taking a snapshot with a small sub-array. Then the target will be positioned at a preset sweet spot on the detector to ensure that the spectral traces fall at the desired position when the GR700XD grism is inserted.

After target acquisition, the GR700XD grism is inserted and exposures can begin. Each exposure will consist in N_I separate integrations (an integration starts with a detector reset) with each integration being as small as *RESET* – *READ* or as large as *RESET*+ N_{read} reads where N_{read} can be as large as 88. We expect to operate at small N_{read} for bright targets. The maximum number of integrations allowed is 65536. As an example, in standard mode, the duty cycle for CDS images is 16.47 sec so an exposure can last up to 300 hours. In bright mode, this duration is ~ 100 hours.

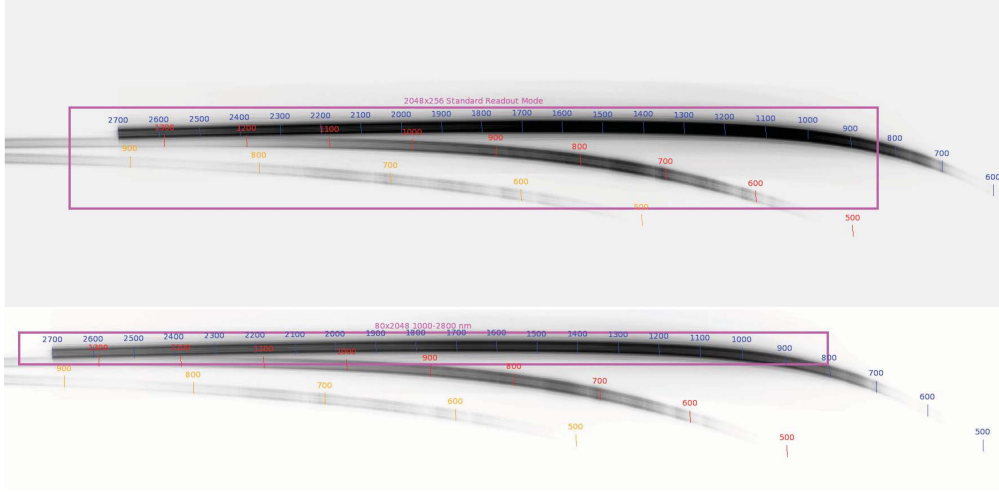


Fig. 18.— *Simulated traces for the SOSS mode with NIRISS in Orders-1 to 3. The zeroth Order is off the detector on the right side. The magenta rectangles represent the 2048×256 (top - standard mode) and 2048×80 (bottom - bright mode) detector sub-arrays read-out for those modes. The standard mode covers from 600 nm to 2800 nm (850 nm to 2800 nm in Order-1, 600 nm to 1350 nm in Order-2) while the bright mode covers from 1000 nm to 2800 nm (in Order-1 only). The Order-3 trace has very low throughput and is unlikely to be of any use. Note that these sub-arrays are along the edge of the detector to make use of the reference pixels and that they are along the amplifier long-axis direction, meaning that the readout can not be multiplexed using 4 amplifiers. The abrupt cut at 2700 nm is an artifact of the simulation.*

7.2.5. Operational Limitations & Efficiency

Wheel repeatability will be the main limitation on the spectral traces position. The encoder precision is equivalent to 0.15° on the wheel which results in a rotation of ~ 4 pixels at each end of the Order-1 trace. Contamination by the Order-2 trace increases from less than 10^{-3} shorter than $2.5 \mu\text{m}$ to $\sim 10^{-2}$ at $2.8 \mu\text{m}$. Otherwise, instrumental scattering was modelled to be at a level smaller than 10^{-3} and is a smooth background contamination. Because the SOSS mode is slitless, another limitation is trace contamination by other stars

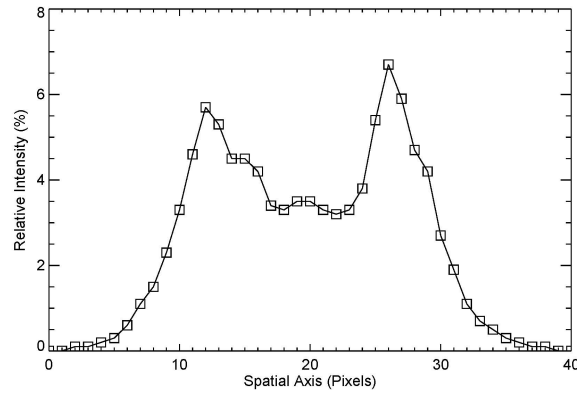


Fig. 19.— *A cut through the spectral trace along the spatial direction near 1.5 microns as measured at cryo vacuum 1 in 2013. The trace is approximately 20 pixels wide with the brightest pixel receiving about 7% of the monochromatic light flux. The trace width does not vary significantly across the wavelength range of 0.6-2.8 microns.*

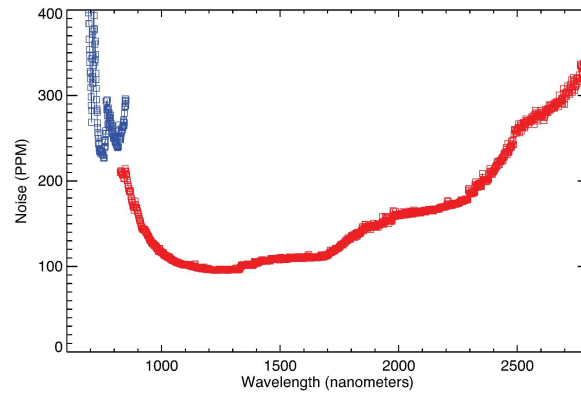


Fig. 20.— *Typical curve of the noise level achieved with NIRISS in its full resolving power on a $J=10$ star for 6 hours of observation.*

in the field. For a given target, contamination by other stars will remain fixed and only change with field rotation as the spacecraft orbits the Sun. So, in a few instances, it may be necessary to schedule the observation to minimize potential contaminants.

7.2.6. Data Simulations

Our simulations were developed for exoplanet transit spectroscopy and secondary eclipse spectroscopy. They are photon-noise limited simulations but include an arbitrary noise floor that we currently set at 20 ppm per bin. They are still 1-D simulations, i.e. the flux is not projected onto a 2-D detector. The instrument throughput is that measured or expected at the beginning of integration (BOI) and includes the optical telescope elements (OTE). No conservative fudge factor is applied to the throughput. The grism in NIRISS will be swapped in the fall of 2014 for one that has a $2 \times (4 \times)$ better throughput in order 1(2). We use this new grism for our simulations. The blaze function used for the new GR700XD grism is that measured in the lab before AR coatings were applied but scaled to account for the presence of an AR coating when the grism is swapped in NIRISS. The main efficiency loss comes from the readout overhead incurred (50% for a reset+read, 33% for a reset+read+read). In addition, an overhead of 10 minutes is assumed for a telescope slew and 20 minutes for the detector to stabilize for a total of 30 minutes wall clock time loss per visit. Figure 20 presents a noise vs. wavelength curve typical of NIRISS, here a J=8.0 star (T=3200 K) observed for 6 hours with a noise floor of 20 ppm.

At the time of this writing, the effect of the intra pixel response (IPR) on the achieved accuracy has not been modelled. NIRISS was designed such that the monochromatic PSF is tilted by ~ 2 degrees (see figure 19), with a spectral trace width of about 20 pixels, that ensures that a spectral line be sampled at about 20 intra-pixel positions and across a full pixel.

Figure 21a presents a transmission spectrum simulation of what we would expect with NIRISS for GJ 1214b, a super-Earth around a star of magnitude J=9.75. The simulation assumes 12 hours of clock time spread over 4 transits, a 20 ppm noise floor. Here, a model (Fortney, private communication) at $50 \times$ solar metallicity and incorporating photochemical

hazes dominated by $0.01 \mu\text{m}$ -sized particles is used. This is a model probably not excluded by the Kreidberg et al. (2014) observations (in the spectral range between 1.1 and $1.7 \mu\text{m}$, the atmosphere signature is almost flat). With NIRISS at the native resolution, individual lines penetrate through the haze. That simulation is of equivalent signal-to-noise ratio as the Kreidberg (2014) observations when binned to the same resolving power. Figure 21b is a simulation of a hot Jupiter, HD189733b for one transit at its actual magnitude of $J=6.1$. Part of the spectrum is missing ($\lambda \leq 1.05\mu\text{m}$) because of the Bright readout mode used to prevent saturation. The third simulation (Figure 21c) is that of an Earth-size planet with *half* its density harbouring a water vapor atmosphere, orbiting a late M star of 3200 K and 0.2 solar radii in its habitable zone. The brightest M star *TESS* will find harbouring an Earth-size transiting planet will likely be $J = 7 - 8$. We set the magnitude to $J = 8.0$ where the standard 256×2048 readout sub-array can be used. Using 5 transits at a resolution binned to $R=70$, our simulation shows that the main ~ 100 ppm features can be detected. For an Earth twin (i.e. with the same density), atmospheric features skrink by a factor of 2 for the same noise level such that detection is at the $\sim 3 - \sigma$ noise threshold. Finally, Figure 21d gives an example of *Secondary eclipse* spectroscopy of LHS 6343 C, an old brown dwarf orbiting an M3 star in the *Kepler* field. NIRISS will easily allow precise spectral typing of this unique brown dwarf for which 4 physical parameters (radius, mass, temperature and luminosity) can be observationally determined.

What can eventually be achieved with NIRISS - be it a low-density Earth-size water world or an actual Earth-twin - is strongly dependent on the noise floor that the instrument will reach. If NIRISS hits 20 ppm (30 ppm is demonstrated with HST) then planets with $\sim 75 - 100$ ppm atmospheric features will be within reach. An exact Earth-twin would require achieveing a floor of better than $\sim 5 - 10$ ppm to detect features at the $3 - \sigma$ level. Work on a NIRISS Optical Simulator (NOS) to better understand the instrumental limitations is starting in the physics laboratory of the Université de Montréal.

7.3. NIRCam

NIRCam consists of 2 identical modules with adjacent fields of view that each cover approximately $2'2'' \times 2'2''$. Each module views the same field through both short wave (SW) and long wave (LW) cameras that are fed via a dichroic beamsplitter with a transition wavelength of $2.4 \mu\text{m}$. The SW cameras are Nyquist sampled at $2.0 \mu\text{m}$ and the LW ones are Nyquist sampled at $4.0 \mu\text{m}$.

NIRCam offers narrow ($R = 100$), medium ($R = 10$), wide ($R = 4$) and double wide ($R = 2$) filters across the $0.7 - 5 \mu\text{m}$ wavelength range. It also features gratings that provide $R \sim 1700$ spectroscopy over the LW $2.4 - 5 \mu\text{m}$ wavelength range with 2 orthogonal dispersion directions per module. These gratings are operated slitlessly, so they are immune to slit losses and any resultant signal modulation during transit observations. The gratings must also be used in series with a filter which selects a portion of the LW spectral region for observation.

NIRCam has a variety of subarray modes to enable observations of bright sources (Table 7). Table 4 gives the L band ($\sim 3.8 \mu\text{m}$) magnitudes for the brightest sources that can be observed with either NIRCam’s the grism or a 32×32 subarray in the filters listed. These saturation limits assume operation up to 80% of full well, or approximately 60,000 e^- . While subarrays are read out using a single amplifier, the H2RGs can also be configured to read out “stripes” of $N_{\text{rows}} \times 2048$ using all four readout amplifiers for still faster frame times.

Three NIRCam modes are likely to be most used for transit, eclipse, and phase curve observations. In-focus imaging will allow photometric measurements of planets with host stars as bright as $K \sim 6 - 8$ mag (Vega system) with a small (32×32 pixel) detector subarray (Table 4). It is possible to image stars $K \sim 6$ mag (Vega) or even brighter when using the +8 wave weak lens (WLP8) in series with a SW filter. The WLP8 lens spreads the light of a star over ~ 130 pixels diameter, reducing the maximum flux per pixel as well as

reducing total photometric fluctuations due to intrapixel response and flat field variations.

Long wavelength (LW) spectroscopy will be conducted using a grism with either the F322W2 (2.4 - 4.0 μm) or F444W (3.9 - 5.0 μm) filter in series; these 2 combinations span the complete NIRCam LW wavelength range. $K \simeq 4$ mag or brighter stars can be observed with the grism when using a 2048×64 detector subarray in striped mode using all 4 output amplifiers.

NIRCam SW and LW arms can observe the same object simultaneously by virtue of the dichroic beamsplitter that divides the light within each module. It is worth noting that current operations plans call for using identical subarrays and identical integration times in the active SW and LW detectors in each module. This should not be a significant issue when observing in basic imaging modes, but there may be some dynamic range issues when imaging in the complementary arm when imaging with the WLP8 lens in the SW side or obtaining grism spectra in the LW side. These issues can be mitigated by selecting modes (filters, weak lens, and/or grism) that produce similar photon fluxes in each wavelength arm. This versatility allows simultaneous SW and LW photometry or SW photometry plus LW spectroscopy. In addition to providing scientific data at 2 wavelengths, this always provides at least one pointing reference. For example, any photometric variations seen in SW images or simultaneous grism spectroscopy could be decorrelated using any measured SW source motion.

The relatively good spatial sampling of the NIRCam optics and the good noise performance of its detectors (similar for NIRISS and NIRSpec as well) will help NIRCam achieve high spectrophotometric precision. The precision of its SW photometry of bright stars can be improved by using the WLP8 lens. The precision of the grism observations may be improved by binning in the dispersion direction, also reducing the effective resolving power below their native $R \sim 1700$ (dispersion $\simeq 1000$ pixels per μm). Thus we expect

that NIRCcam will achieve spectrophotometric precision similar to that of *HST* WFC3 G141 data, ~ 35 ppm (Knutson et al. 2014) even though *JWST* lacks the fast scanning mode that has been implemented for the *HST* observations.

After the discussion of instrument constraints on transit observations at the workshop, the NIRCcam team discovered a software limitation to the duration of a single exposure of just 9.1 hours. Once identified, this limit is now being increased to a value of at least 48 hr.

7.4. MIRI

MIRI provides modes for imaging, coronagraphic imaging, low resolution ($R \sim 100$), and integral field moderate resolution ($R \sim 2000$) spectroscopy using three Si:As 1024×1024 pixel detector arrays. The MIRI imaging module (MIRIM) optics provide a $74'' \times 113''$ field of view with a scale of $0''.11$ per pixel. The MIRIM has 10 selectable filters with central wavelengths $5.6 - 25.5 \mu\text{m}$ and bandwidths of $0.7 - 4.6 \mu\text{m}$ (Bouchet et al. 2015). The low resolution spectrograph (LRS) provides slit or slitless $R \sim 100$ spectra from 5 to $\sim 12 \mu\text{m}$ via a double (compound) prism in the MIRIM filter wheel (Kendrew et al. 2015). MIRIM also provides 3 four quadrant phase mask coronagraphic fields spanning central wavelengths from $10.65 - 15.5 \mu\text{m}$ and a Lyot coronagraph that operates at $23 \mu\text{m}$ (Boccaletti et al. 2015). A single 1024×1024 pixel Si:As IBC detector array collects photons from all of the MIRIM modes, and two similar detectors are used in the MIRI medium resolution spectrograph (MRS) (see Rieke et al. 2015). The MRS fields are as large as $7''.7 \times 7''.7$, and they are located adjacent to the MIRIM field. The MRS operates at $R = 1300 - 3700$, and its two detector arrays see approximately one third of its $\lambda = 5 - 28 \mu\text{m}$ spectral coverage at any given time (Wells et al. 2015). MIRIM imaging and slitless LRS photon conversion efficiencies are on the order of 0.3, and detailed MIRI sensitivity calculations are presented in Glasse et al. (2015).

Three MIRI modes will likely be most useful for transit, eclipse, and phase curve science: MIRIM photometry, low-resolution slitless spectroscopy with the LRS, and medium-resolution integral-field spectroscopy with the MRS. Spectra obtained in MRS mode are interleaved, meaning that 3 separate observations are required to obtain a continuous spectrum over its $5 - 28 \mu\text{m}$ range (Fig. 14). Given the complexities of diffraction, potential slicer and slit losses, detector undersampling & fringing, and considering the difficulties experienced in past transit observations with integral field instruments (e.g., Angerhausen et al. 2006), the MRS mode is unlikely to be useful for obtaining exoplanet spectra over a broad wavelength range with high spectrophotometric precision. However, it may be that focused observations of narrow lines using only a single dichroic/grating setting are tractable. Furthermore, MRS is the only option for spectroscopy beyond $\sim 12 \mu\text{m}$.

MIRI has a variety of sub-array modes that enable a bright sources to be observed in a variety of instrument configurations (Table 8) with saturation magnitudes given in Table 4. The bright limits for imaging, slitless LRS, and MRS modes are in the $K = 4 - 6$ mag range for late-type host stars. These values are calculated for using subarrays with 2 frames per integration (RESET – READ – READ sequence). There is a chance that more frames will need to be acquired in each MIRI integration in order to minimize systematic detector noise, and these bright limits would be impacted if this occurs (e.g., 0.75 mag fainter if 4 frames are required per integration).

The LRS uses a $0.5''$ slit to provide $R \sim 70$ spectroscopy from $5-12 \mu\text{m}$. However, it can also be operated in a slitless mode by positioning the source in the field of the Lyot coronagraph region with the LRS double prism selected in the MIRI filter wheel. This will prevent slit losses and their resultant time-correlated variability in time-series spectroscopy. This spatial location of the star also allows use of the SLITLESSPRISM detector subarray, shortening the minimum integration time to provide the high flux bright limit given in

Table 4. Like the MIRI Imager, the LRS PSF is spatially undersampled at wavelengths $\lambda \lesssim 7\mu\text{m}$, so there may be variations in the signal correlated with pointing motions due to intrapixel sensitivity variations (as were seen in many *Spitzer*/IRAC observations). This challenge can likely be addressed to ensure that MIRI exhibits a noise floor at least as good as that of *Spitzer* (≤ 50 ppm, §4.3.1) given the similarity of their Si:As detectors. Considerable work remains to be done on the planning of MIRI observations and in the development of the MIRI detector pipeline, and hopefully this work will improve the actual noise floor achieved.

Finally, MIRI provides photometry via a set of 10 non-coronagraphic filters over the $5 - 28\mu\text{m}$ range with bandwidths in the range $R = 3.5 - 10$. As for the LRS, the MIRI imager PSF is undersampled at $\lambda \lesssim 7\mu\text{m}$, so intrapixel sensitivity variations may impact the spectrophotometric precision of data at those wavelengths. The PSF shows a characteristic “cross”-like shape due to regularities in the array substrate, but standard aperture and/or PSF-fitting photometry should adequately deal with this. MIRI may be the best instrument for detecting the thermal emissions of cool planets due to its long wavelength coverage.

8. Illustrative Science Programs and Cross Instrument Opportunities

The Workshop presenters discussed a large number of potential programs involving observations with more than one instrument, including possible early-science and/or Guaranteed Time projects. For gas giants (hot Jupiters down to sub-Neptunes), there was general agreement that early observations should focus on full wavelength coverage, with low- to medium-resolution reconnaissance spectroscopy ($R=100-1000$) of a modest subset of targets plus a smaller number of targets to be studied at higher spectral resolution ($R>1000$). Illustrative targets (including a nearby super-Earth that might be discovered by TESS) and observing setups are described in detail in Appendix 2. Appendix 3 and

Appendix 4 give the SNR at representative wavelengths and resolutions after a single transit or phase curve measurement. For objects like GJ1214b for which the single transit SNR will be low at some spectral resolutions, it will be necessary to increase the SNR by either degrading the spectral resolution and/or coadding multiple transits.

JWST generally requires ~ 4 transits or occultations to assemble a continuous, moderate-resolution spectrum from 0.6–12 μm . Such a program would likely use NIRISS (0.6–2.5 μm), NIRCам (2.4–5.0 μm), and MIRI (5–12 μm) and would be limited to targets with $J > 6 - 8$ mag (see Table 4). Some of the best-known targets like HD 209458b, HD 189733b, and GJ 436b are right at the saturation boundary necessitating careful assessment of saturation limits at each wavelength, but many interesting targets such as GJ 3470b, WASP-43b, WASP-12b are still adequately bright for easy observation and will not present any saturation problems. For stars fainter than about $J > 11$ mag it would be possible to use just two modes for full wavelength coverage NIRSpec/CLEAR/PRISM and MIRI/LRS. By using its 4 amplifier, striping readout mode, NIRCам spectroscopy is possible for stars as bright as $L \sim 3$ mag, thereby recovering some of the brightest targets (Table 4).

Once the limiting capabilities of *JWST*'s instruments are understood after the first year of operation, there will be time in General Observer Cycles 2 and beyond to undertake more ambitious programs. *JWST*'s large collecting area means that many large planets, e.g. gas and ice giants, can be measured with medium to high resolution spectroscopy in just a single transit, and observed with complete wavelength coverage, in just 2-4 transits, depending on the selection of instrument modes and primary vs. secondary transits, etc. A spectroscopic survey of 100-200 planets, covering masses from 0.05 to 5 M_{Jup} , metallicities, [Fe/H], from -0.5 to 0.5, and host masses from M5V-F5V would be possible, albeit with a major commitment of observing time. Assuming a sample of 150 planets with an average

observation duration of 6 hours (2 hr for the transit plus 4 hr for stellar baseline) and each system observed in 4 different instrument modes, then a survey would require roughly 3600 hr. But by determining elemental abundances and other properties across such a broad range of stellar properties, we would obtain a dataset which would revolutionize our understanding of planet formation. Mini-Neptunes and Super-Earths ($0.015 - 0.05M_{Jup}$ or $5 - 15M_{\oplus}$) could be addressed in this same way around lower mass stars. A sample of 50 suitable targets is predicted to come from *TESS* (§3) and might require an additional 1200 hr of *JWST* spectroscopy.

Programs challenging *JWST*'s ultimate levels of precision should also be carried out, e.g. detection H_2O , CO_2 , or O_3 via transmission or emission spectroscopy from potentially (or nearly) habitable super-Earths (Kaltenegger & Traub 2009; Deming et al. 2009). The participants agreed that attempts to predict the feasibility of these observations are highly dependent on the systematic-noise floors of the instruments. Early observations of bright objects are best-suited to characterize these floors – until then, simple extrapolations from the instrument Exposure Time Calculators should be treated with caution. If such programs are feasible it is clear that they will require a significant amount of telescope time because many transits must be observed to build up SNR. *TESS* targets will be critical for this program which will require discovery of small planets orbiting bright stars.

JWST's enhanced sensitivity also renders feasible with one or two transits projects that on *Spitzer* required the stacking of many such events. For example, the first 2D map of a hot Jupiter's day side required seven secondary eclipses with *Spitzer*/IRAC at $8\mu m$ (Majeau et al. 2012b; de Wit et al. 2012b). *JWST*'s collecting area is $\sim 56\times$ that of *Spitzer* for an SNR increase of $7-8\times$. In principle MIRI photometry of HD 189733b or a comparable target could generate a dayside map with just a single secondary eclipse. If correlated noise can be sufficiently controlled, *JWST* may enable eclipse maps at shorter wavelengths

(for hot planets) for cooler planets (at longer wavelengths), or perhaps even spectroscopic eclipse maps. Moreover, the smaller number of eclipses required to satisfactorily observe an object makes it more likely that time will be available to use multiple instruments and multiple modes on a single target.

9. Engage the Community

9.1. Data Processing Challenges and Simulations

The reliable reduction of transit, eclipse or phase curve observations is an enormously challenging task. Transit observations involve doing exactly what one’s college physics teacher said never to do, namely subtract two big numbers and look for small differences. In the case of transits, we are looking for differences as small as 10 ppm with observations spanning many hours or even days. Every aspect of the stellar host (starspots, variability, confusing effects of its spectrum), the telescope (pointing and focus drifts), the instrument and detectors (numerous bad habits as described in §6), and post-processing software (over or under-correcting for instrumental effects, developing appropriate measurement uncertainties) must be well characterized and validated.

JWST will provide both planning tools and data processing tools optimized for transit observations. To plan transit observations, specific observing templates will be available for each of the science instruments. These templates are being designed to yield the highest-possible photometric stability by minimizing disturbances to detector readout operations and to the various observatory systems.

Once the data have been collected, the raw data will be available in the archive and the JWST pipeline will provide processed single-integration images. It is expected that the science community will play a key role in extracting the ultimate precision from transit

data, as it has for data acquired using Hubble and Spitzer. The science operations center will work with the community to incorporate best practices into the pipeline over time, and to provide any additional information that may be needed to maximize the science return from transit observations.

To enable rapid and reliable reduction of transit observations, observers must have access to a broad range of *JWST* data to be able to track the state of the instrument over long periods and to be able to place each observation in context. For example, a large amount of data and detailed analysis was required to characterize *HST*/WFC3 instrumental effects and to construct the *Spitzer*/IRAC pixel phase maps. It will be essential to be able to download large amounts of *JWST* data, something for which existing interfaces to mission archives are often not optimized, e.g. extract all NIRSPEC observations of stars of some magnitude and spectral type or to track the evolution of the flat-field response.

The community should be encouraged, perhaps in a coordinated way through the STScI, to participate in end-to-end simulations to quantify the impact of instrument, pipeline and analysis tools on retrieved exoplanet characteristics. Once *JWST* is in orbit, null-test observations should be carried out very early on for each instrument/mode and made available to the community for detailed analysis. e.g., an exoplanet transit “null-test” over 8 hours or a phase-curve “null-test” over 4 days would be of great value in developing post-processing tools.

In developing observational sequences and pipeline tools optimized for transits, STScI should incorporate “lessons-learned” from current instruments, e.g. the ramp effect, detector noise, inter- and intra-pixel sensitivity variations, and be ready to calibrate and validate reduction and post-processing tools. It will be important to develop a consensus on the best methods to remove these effects. Ground testing can help identify specific detector or instrument issues early. By engaging the community in activities before and immediately

after launch, the community will be ready to submit well-founded proposals and to optimize the early return of exciting science from *JWST*.

Once reliable data are in hand, a second level of challenges awaits, namely the retrieval of physical parameters such as abundances of various atomic and molecular species, vertical and horizontal temperature structure in the atmosphere. As noted by Hansen et al. (2014), a proper treatment of the observational uncertainties in *Spitzer* photometry make it impossible to distinguish in a Bayesian sense between a complex atmospheric model and a simpler blackbody model. *JWST*'s higher SNR photometry or, better yet, multi-wavelength spectroscopic data should greatly improve the interpretative power of the models, but the caution remains. A community effort to agree on a set of test observations to analyze and compare the derived parameters for consistency and accuracy would give the community confidence that reliable results can be obtained from *JWST*'s observations.

9.2. Obtaining Transit Observations Soon After Launch

As noted in the previous section, workshop participants (both instrument team members and potential General Observers) felt strongly that early access to *JWST* data would be very important for learning how to work with transit observations. Analysis of this early data would inform modifications to data acquisition processes, the development of pipelines and post-processing tools, and improve the quality of proposals for Cycle 2 and beyond.

Such initial transit observations may potentially come from Early Release Observations (ERO), Science Verification (SV) datasets, and/or the Early Release Science Program (ERS). However, the objectives of each of these three classes of observation are distinct:

- *Early Release Observations.* As defined by NASA-SMD policy, “Early Release

Observations (EROs) will be taken by *JWST* during both the commissioning and post-commissioning phases of operation. These observations will be chosen to have wide public appeal and are designed to demonstrate the capabilities of the *JWST* instruments. Publication or reporting in any form of results of these observations is embargoed until the EROs are released. The ERO data become publicly available at that time” (NASA-SMD Policies and Guidelines for the Operations of the James Webb Space Telescope at the Space Telescope Science Institute, Policy 4). Thus, as noted by the *JWST* Advisory Committee (JSTAC⁷), the ERO program “is a public media activity to demonstrate early mission success. The ERO data will be useful for science, but their primary purpose is a media demonstration that the mission is operational and on track to begin its science program” (JSTAC, March 2014).

- *Science Verification (SV)* datasets will be taken during the six month commissioning period after launch and are designed to confirm the basic capabilities of the science instruments in the context of observatory operations. They are likely to offer limited opportunities for science observations. The SV datasets will also be embargoed from public access until the release of the EROs.
- *The Early Release Science (ERS) Program* was recommended by the JSTAC to “to enable the community to understand the performance of *JWST* prior to the submission of the first post-launch Cycle 2 proposals that will be submitted just months after the end of commissioning. To meet this goal, science data need to be released as soon as commissioning activities allow. The data would complement the Early Release Observations (ERO) and the Science Verification (SV) datasets [and] should have no proprietary period. The JSTAC recommends that these data be released both in raw form and with any initial calibrations as soon as possible; the

⁷<http://www.stsci.edu/jwst/advisory-committee>

key aspect is speed” (JSTAC, June 2010). While the size and scope of this program are still undefined, the program will be supported by Director’s Discretionary Time. Over the next two years, STScI will work with Guaranteed Time Observers and the community to plan for implementation of ERS observations, “so that the community involvement in the selection of targets, science objectives and modes is carried out efficiently and is completed when needed before the Cycle 1 Call for Proposals” (JSTAC, March 2014).

Given the scope of each of these programs, the ERS program likely provides the best chance for the community to secure the early transit observations that it needs to maximize exoplanet science with JWST. Workshop participants were greatly in favor of such an approach, and were eager to learn more about how to help define the ERS to ensure that key transit observations are represented in its portfolio of observations. Participants also emphasized that transit-related observations should be taken as early as possible in the mission to quickly determine instrument performance in a few key modes.

The participants urge the project, the instrument teams, and STScI (along with relevant advisory bodies) to take these urgent recommendations into consideration as they plan various early observations with JWST.

10. Conclusions

The *JWST* Transit Workshop drew together exoplanet observers, modelers and theoreticians, experts in instruments currently making transit observations, and experts in the *JWST* observatory, its instruments and science operations. The goals of the meeting were to provide a forum where the exoplanet community could come together with representatives of *JWST* to learn about the capabilities of *JWST* for transit science, to form

ideas for ambitious, yet feasible, observational programs, and to pass on lessons-learned from previous missions. Some of the most important conclusions are listed below. More detailed information is available in individual presentations available at the Workshop website⁸.

- All the workshop participants were excited at the prospect of bringing the dramatic new capabilities of JWST, in particular its large collecting area, stable orbit, broad wavelength coverage and spectral resolution, to bear on a wide variety of exoplanet topics.
- A large sample of exoplanets orbiting bright stars will be available for study from space-based (Kepler, Kepler/K2, TESS, and CHEOPS) as well as ground-based surveys.
- The validation of these planets, the characterization of their bulk properties, and the accurate determination of their orbital parameters will require a major commitment by ground-based community, supported by NASA, to obtain low and high precision radial velocity as well as adaptive optics imaging.
- A complete science program over the lifetime of *JWST* will involve observing wide variety of planets.
 - A survey of 100-200 gas and ice giants with a range masses ($0.05-5 M_{Jup}$) orbiting stars with a broad range of spectral types, metallicity would lead to a transformational breakthrough in our understanding of the formation and evolution of planets. Transit signals are strong enough that a single transit/instrument mode should provide adequate sensitivity in almost all cases.

⁸<http://nexsci.caltech.edu/committees/JWST/agenda.shtml>

- The study of a few 10s of mini-Neptunes or super-Earths ($5\text{-}15 M_{Jup}$) would explore a species of planet not found in our own solar system in a variety of stellar environments. In many cases, observations of these smaller planets could be accomplished in a single transit/per mode for planets orbiting M stars.
- Intensive observations of one or two terrestrial-sized planets ($1\text{-}5 M_{\oplus}$), preferably located in the Habitable Zone of their host stars, might only be possible with filter photometry and might require coadding many 10s of transit observations. But such observations would offer the promise of characterizing the atmospheres of a planet much like our own.
- Many individual planets will have properties worthy of careful study, e.g following the phase curve of a highly eccentric planet through periastron passage to explore atmospheric chemistry dynamics under drastic changes in insolation, making two dimensional tomographic maps of planetary atmospheres using high cadence, high SNR observations, etc.
- A complete multi-wavelength dataset for each object in either primary transit or secondary eclipse will require between 2 and 4 separate observations using various instrument modes. Each transit observation will require between 5 and 20 hours while full phase curve coverage will require between 2-4 days of uninterrupted observation.
- Experience from *Kepler*, *Spitzer*, and *HST* shows that the acquisition of transit data requires careful operational design to ensure maximum stability of every aspect of *JWST* for many hours or even days. The project is urged to work with the instrument teams and other experts to understand proposed instrument sequences in great detail and to develop on-orbit tests as early as possible in the mission. Among the lessons-learned from *HST*, *Kepler* and *Spitzer* are the following:
 - Strive to reduce spacecraft interruptions to an absolute minimum during

hours-long, or even days-long, transit or phase curve observations. Even small disturbances from heaters, reaction wheels, or discontinuous pointing shifts can have significant effects at the level of a $\gg 10$ s of ppm.

- Recognize the complexity of scheduling a large number of highly time constrained events.
- Identify detector “sweet spots” early in the mission to make it possible to characterize a small number of pixels in exquisite detail for all transit observations in a particular instrument mode. Ensure that appropriate operating modes are available to take advantage of these “sweet spots”.
- Given the large amount of effort required to develop on-orbit data acquisition procedures, calibration techniques and post-processing tools for even a few instrument modes, STScI should encourage early identification of a few preferred modes for each instrument. As experience is gained, additional configurations could be supported as well. While this recommendation should not be construed as restricting the community from developing innovative new techniques, e.g. scanning a source with HST/WFC3, *JWST* has a limited lifetime and diluting the effort with a plethora of modes could prove detrimental.
- Experience from *Kepler*, *Spitzer*, and *HST* shows that the pipeline and post-processing of transit data require careful calibration and algorithm development. STScI is urged to work with the instrument teams and transit experts to understand the pipelines and requisite calibration parameters in great detail.
- Prelaunch measurements using either the flight instruments themselves or specialized testbeds can provide important insights to detector and instrument performance.
- Engage the exoplanet community in the years before launch and soon after launch with data challenges and access to a small amount of transit data taken early in

the mission to enable rapid development of optimized observing practices and data reduction tools. Many of the highest precision observing sequences and tools used with *HST* and *Spitzer* data were developed by the observer community working in close collaboration with science center personnel.

JWST will provide dramatic new capabilities for improving our understanding of planetary systems, including gas and ice giants, mini-Neptunes and Super-Earths, and even Earth-sized planets in the habitable zones of their host stars. Careful preparation in advance of launch by the instrument teams, the project, and STScI, coupled with a deepened awareness of JWST’s capabilities within the exoplanet community, should bring about a dramatic new era of exoplanet exploration.

11. Acknowledgements

The Principal Investigators and members of each instrument team, as well as STScI and *JWST* Project personnel all gave generously of their time to make this workshop a success. CAB would like to thank Ms. Ellen O’Leary and other NExSci personnel for their invaluable support for all aspects of the workshop. People wishing to cite aspects of this Workshop are encouraged to cite individual presentations (Table Appendix 1) as given at the “Caltech *JWST* Transit Workshop, March 2014”. Some of the research described in this publication was carried out in part at the Jet Propulsion Laboratory, California Institute of Technology, under a contract with the National Aeronautics and Space Administration. Copyright 2014 California Inst of Technology. All rights reserved.

Table 3. Extract of Spitzer FITS Header Illustrating Multiple Timestamps

Quantity	Value	Comments
DATE_OBS	2009-01-28T08:16:46.745	Date & time (<i>UTC</i>) at DCE start
UTCS_OBS	286402606.745	[sec] DCE start time from noon, Jan 1, 2000
UTCMJD_OBS	54859.3449855	[days] Mod. Julian Date (<i>MJD</i>) in <i>UTC</i> at DCE start (=JD-2400000.5)
HMJD_OBS	54859.3462516	[days] Corresponding Helioc. Mod. Julian Date
BMJD_OBS	54859.3462694	[days] Solar System Barycenter Mod. Julian Date
ET_OBS	286402672.929	[sec] DCE start time (<i>TDB</i> seconds past J2000)
SCLK_OBS	917598037.993	[sec] SCLK time (since 1/1/1980) at DCE start

Table 4. Brightness Limits for Various Instrument Modes

Instrument	Mode	Brightness Limit (mag) ^a
NIRSpec		
	Low-resolution spectroscopy	$J > 11$
	Medium-resolution spectroscopy	$J \gtrsim 6$ (best-case)
NIRISS		
	Standard spectroscopy	$J > 8.1$
	Subarray spectroscopy	$J > 6.9$
NIRCam		
	L (mag) limits	
	Long-wavelength spectroscopy	32×2048 Subarray
	F277W	3.7
	F322W2	3.7
	F356W	3.8
	F410M	3.8
	F444W	3.8
	Photometry	64×64 Subarray
	F277W	9.2
	F322W2	10.0
	F356W	9.3
	F410M	8.2
	F444W	9.2
MIRI		
	8 μm imaging (F770W)	$K > 6$
	15 μm imaging (F1500W)	$K > 3 - 4$
	LRS Spectroscopy	$K > 3 - 4$

^aFor integrations with NFRAMES=1, NGROUPS=2.

NIRSpec transit spectroscopy				
Instrument mode	SLIT/A1600			
Aperture size (projected on the sky)	1.6" × 1.6"			
Aperture size (projected on the detectors)	~16 × 16 pixels			
Low spectral resolution spectroscopy (R~100)				
Wavelength range:	from 0.6 μm to 5.3 μm in a single band			
Spectral resolution:	30-300			
Instrument configuration:	CLEAR/PRISM			
Readout window size:	512 × 32 pixels (spectral × spatial)			
Medium spectral resolution spectroscopy (R~1000)				
Instrument configuration:	Range	Resolution	Readout window size	
F070LP/G140M	[0.7 μm , 1.2 μm]	500-850	2048 × 32 pixels	
F100LP/G140M	[1.0 μm , 1.8 μm]	700-1300	2048 × 32 pixels	
F170LP/G235M	[1.7 μm , 3.1 μm]	700-1300	2048 × 32 pixels	
F290LP/G395M	[2.9 μm , 5.2 μm]	700-1300	2048 × 32 pixels	
High spectral resolution spectroscopy (R~2700)				
Instrument configuration:	Range	Resolution	Readout window size	
F070LP/G140H	[0.7 μm , 1.2 μm]	1300-2300	2048 × 32 pixels	
F100LP/G140H	[1.0 μm , 1.8 μm]	1900-3600	2048 × 32 pixels	
F170LP/G235M	[1.7 μm , 3.1 μm]	1900-3600	2048 × 32 pixels	
F290LP/G395H	[2.9 μm , 5.2 μm]	1900-3600	2048 × 32 pixels	

Table 5: Characteristics of the NIRSpec/A1600 mode for transit spectroscopy.

Noise contribution	Description	Comment
Detector and shot noises	These contribution are included in the baseline simulations and used to estimate the "noise floor".	Used as a benchmark.
Variable aperture losses	The level of aperture losses can change when the source drifts during a transit observation.	Raw contribution of typically 40 ppm (B. Dorner, PhD thesis, 2012).
Intra-pixel sensitivity changes	The response of the detectors can change when the source drifts during a transit observation.	Raw contribution of up to 400 ppm. Major contributor because of the poor PSF sampling in NIRSpec.
Accuracy of the flat-field correction	Another source of detector response change when the source drifts during a transit observation.	Raw impact not yet assessed.
PSF variations	The signal amplitude will change as the footprint of the PSF on the detectors change.	Raw impact not yet assessed.
Persistence	Residual signal changing with time.	Observed in <i>HST</i> /WFC3 data (e.g. Berta et al. 2012).

Table 6: List of various noise contributions for the NIRSpec transit spectroscopy.

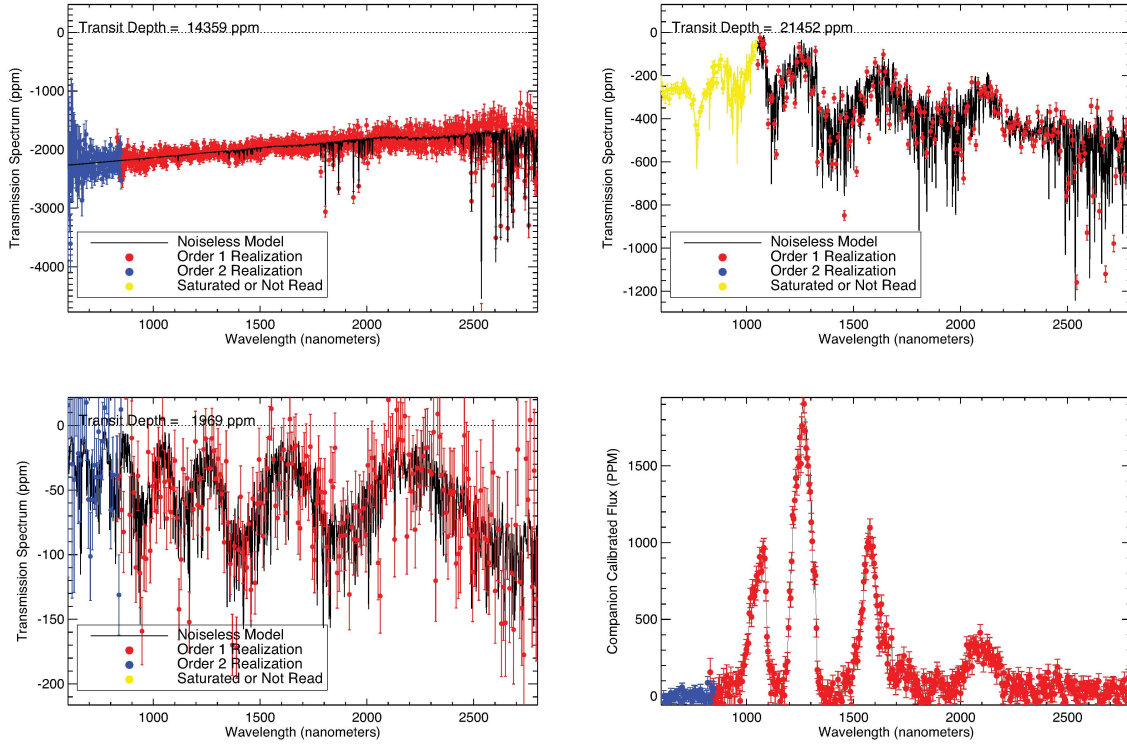


Fig. 21.— *top,left)* Simulation of GJ 1214b observed with NIRISS for a $50\times$ solar atmosphere with haze (model from J. Fortney). This simulation assumes 12 hours of clock time spent over 4 transits. At the native NIRISS resolution, individual lines penetrate the haze despite the very flat spectrum up to $1.7\mu\text{m}$. *top,right)* Simulation of HD189733b observed with NIRISS. This target requires 6.5 hours of clock time if a slew+detector stabilization overhead of 30 minutes is assumed and twice the amount of time is spent out of transit as in-transit. To prevent saturation, a reset+read mode is used rather than a reset+read+read mode. *bottom, left)* Simulation of an Earth-size water world planet with half the Earth’s density observed with NIRISS. We stack 5 transits and assume $J=8.0$ for a late M (3200 K) star of 0.2 Sun radii orbiting in the habitable zone. This target requires 32 hours of clock time if a slew+detector stabilization overhead of 30 minutes is assumed and twice the amount of time is spent out of transit as in-transit. *bottom,right)* Secondary eclipse simulation of the brown dwarf LHS 6343 C observed with NIRISS. A single secondary eclipse (5 hours of clock time) delivers a high quality spectrum allowing precise spectral typing to determine the brown dwarf temperature and thus constrain observationally the radius, mass, temperature and luminosity.

Table 7. NIRCcam Subarray Modes for Transits

Size (pixels)	FOV (")		Frame	Comment
	Short Wave	Long Wave	Time	
64×64	2.05	4.16	49.4ms	in-focus photometry
160×160	5.12	10.4	277ms	defocused SW photometry
400×400	12.8	26.0	1.652s	defocused SW + long events
2048×32	N/A	133×2.1	173ms	(TBC) LW grism spectroscopy
2048×320	N/A	133×10.2	1.682s	(TBC) LW grism + defocused SW
2048×2048	65.3	133	10.74s	Faint host stars; long events

Table 8. Properties of MIRI Subarray for Transits

Subarray Size	Subarray Size Columns×Rows	FAST Frame Time	Max Flux	Max Flux
		(sec)	F560W [mJy]	F2550W [mJy]
FULL	1032x1024	2.775	17	360
BRIGHTSKY*	968x512	1.326	34	780
SUB256*	668x256	0.507	90	2150
SUB128	136x128	0.119	370	8400
SUB64	72x64	0.085	520	12000
SLITLESSPRISM	72x416	0.159	3000 using P750L at 7.5 μ m	
MASK1065	288x224	0.24	3000 using P750L at 7.5 μ m	

Note. — *Only available if Burst mode provides acceptable operation

A. Meeting Agenda and Attendees

Table Appendix 1. Meeting Agenda

Topic	Speaker
DAY 1: March 11, 2014	
Topic	Speaker
<i>Goals of Meeting</i>	C. Beichman& J. Lunine
<i>Key Science Opportunities</i>	
Spectroscopy of Giant Planets	J. Fortney
Spectroscopy of Super Earths	E. Kempton
Atmospheric Dynamics and weather. Full phase coverage	H. Knutson
Transit Photometry	D. Deming
Frontiers of Precision Exoplanet Atmosphere	L. Kreidberg
Characterization with HST	
<i>Transit Best Practices</i>	
HST Best Performance and Best Practices	D. Sing
Hot Jupiter Spectroscopy wth HST/WFC3	A. Mandell
Kepler Best Performance and Best Practices	J. Christiansen
Spitzer Best Performance and Best Practices	S. Carey & Ian Crossfield
Lessons from Spitzer Spectroscopy	J. Bouwman
<i>JWST Operations Issues for Transits</i>	M. Clampin & J. Stansberry
<i>Detector Problems and Features</i>	
HgCdTe/ASIC HgCdTe Detectors	Marcia Rieke
Silicon detectors	M. Ressler
Challenges in Measurement Repeatability	M. Swain
DAY 2: March 12, 2014	
<i>Targets for JWST</i>	
Ground RV/transits	J. Bean
Kepler and K2	S. Howell
TESS	G. Ricker & D. Latham
M Stars as JWST Targets	C. Dressing
CHEOPS	D. Ehrenreich
GAIA	A. Sozzetti
Precursor Data Needs	D. Ciardi
Challenge of Stellar Variability	P. McCullough

Table Appendix 1—Continued

Topic	Speaker
<i>Instrument modes for transits</i>	
NIRSPEC	P. Ferruit & S. Birkmann
NIRISS	R. Doyon & L. Albert
NIRCam	T. Greene
MIRI	T. Greene & P.-O. Lagage
DAY 3: March 13, 2014	
<i>Data Processing challenges and requirements</i>	
What is the Smallest Planetary Atmosphere JWST Will Characterize?	D. Deming
Laboratory Testbeds	Gautam Vasisht & C. Beichman
Pipeline Data Processing Challenges	P. Deroo
<i>Engage the Community</i>	
Science Timeline for JWST	J.Lee
Data Simulations	S. Birkmann& J. Valenti

Workshop Attendees	
Name	Email Address
Loic Albert	albert@astro.umontreal.ca
Jacob Bean	jbean@oddjjob.uchicago.edu
Charles Beichman	chas@ipac.caltech.edu
Bjoern Benneke	bbenneke@caltech.edu
Stephan Birkmann	Stephan.Birkmann@esa.int
Gary Blackwood	gary.h.blackwood@jpl.nasa.gov
Jeroen Bouwman	bouwman@mpia-hd.mpg.de
Sean Carey	carey@ipac.caltech.edu
Jessie Christiansen	christia@ipac.caltech.edu
David Ciardi	ciardi@ipac.caltech.edu
Mark Clampin	mark.clampin-1@nasa.gov
Ian Crossfield	ianc@jpl.arizona.edu
Drake Deming	lddeming@gmail.com
Pieter D. Deroo	pieter.d.deroo@jpl.nasa.gov
Jean-Michel Desert	desert@colorado.edu
Rene Doyon	doyon@ASTRO.UMontreal.CA
Courtney Dressing	cdressing@cfa.harvard.edu
Pierre Ferruit	pferruit@rssi.esa.int
Jonathan Fortney	jfortney@ucolick.org
Paul Goudfrooij	goudfroo@stsci.edu
Tom Greene	tom.greene@nasa.gov
Matthew Greenhouse	matthew.a.greenhouse@nasa.gov
Dean Hines	hines@stsci.edu
Steve Howell	steve.b.howell@nasa.gov
Name	Email Address
Eliza Kempton	kempton@grinnell.edu
Tony Keyes	keyes@stsci.edu
Heather Knutson	hknutson@caltech.edu
Laura Kreidberg	kreidberg@uchicago.edu
Jessica Krick	jkrick@caltech.edu
David Lafrenière	david@ASTRO.UMontreal.CA
Pierre Olivier Lagage	pierre-olivier.lagage@cea.fr
David Latham	dlatham@cfa.harvard.edu
Janice Lee	jlee@stsci.edu
Jonathan Lunine	jlunine@astro.cornell.edu
Avi Mandell	Avi.Mandell@nasa.gov
Peter McCullough	pmcc@stsci.edu
Michael E. Ressler	michael.e.ressler@jpl.nasa.gov
George Ricker	grr@space.mit.edu
Marcia Rieke	mrieke@as.arizona.edu
Massimo Robberto	robberto@stsci.edu
Avi Shporer	shporer@gps.caltech.edu
David Sing	sing@astro.ex.ac.uk
Roger Smith	rsmit@astro.caltech.edu
Alessandro Sozzetti	sozzetti@oato.inaf.it
John Stansberry	jstans@stsci.edu
Mark Swain	mark.r.swain@jpl.nasa.gov
Jeff Valenti	valenti@stsci.edu
Gautam Vasisht	gv@s383.jpl.nasa.gov

Table Appendix 2: Workshop Attendees

B. Detector Operations

The *JWST* standard for specifying and acquiring science exposures is called "MULTIACCUM". MULTIACCUM exposures consist of one or more sample-up-the-ramp *integrations*, each integration is composed of one or more *groups*, while each group is made up of one or more *frames* (i.e. non-destructive reads of the signal on each pixel). In order to limit data rates, the frames from within a group can be co-added before being stored on the solid-state recorder (SSR). The overall science exposure scheme is illustrated for a simple example in Figure 22. Terms and definitions are given in Appendix B, Table 9.

Exposure commands are issued by the on-board scripts subsystem (OSS), are received and translated by the flight software (FSW) for the specified science instrument (SI). For the three instruments (NIRCam, NIRISS and NIRSpec) using the $2k \times 2k$ HgCdTe (H2RG) detectors, the exposure parameters are then sent to ASIICs (application specific integrated circuits) that are co-located with the detectors. Each ASIC controls, and digitize the data from, a single H2RG detector. Once an ASIC receives the exposure parameters and the signal to start an exposure, it executes that exposure autonomously without further intervention from SI FSW or from OSS. The 3 MIRI Si:As detectors are interfaced to warm focal plane electronics (FPE) boards that control the detectors' biases, operate their clocks, and also amplify and digitize their signals.

As of this writing, both reads and resets (during which accumulated signal on the detectors is cleared out) are performed on a pixel-by-pixel basis. The time to acquire a read, or to reset all the pixels, depends primarily on the number of pixels configured to be addressed. Small overheads are incurred when telemetry from the ASIC is inserted into the data stream. The time to acquire one frame of data is given by:

$$T_{Frame} = \left(\frac{N_{COL}}{N_{output}} + 12 \right) \times (N_{ROW} + 1) \times 10\mu\text{sec}$$

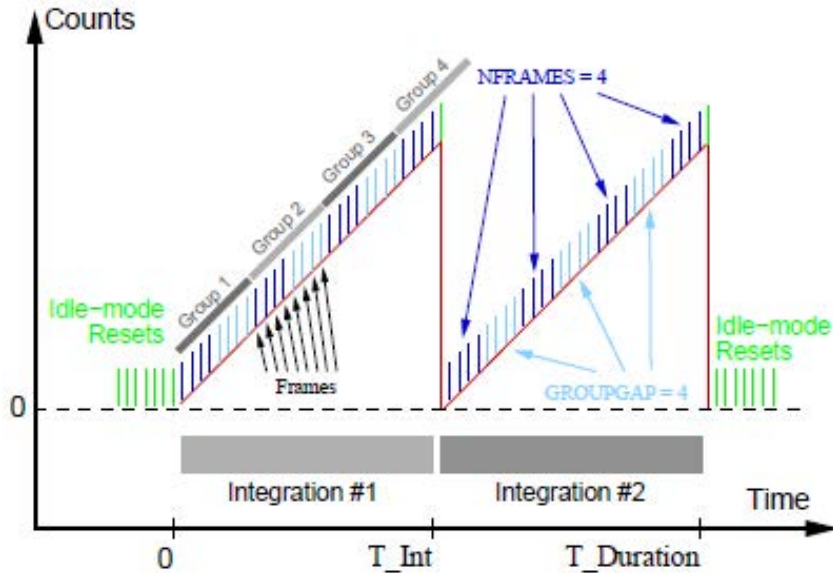


Fig. 22.— Schematic showing an example of a possible MULTIACCUM exposure consisting of two integrations ($NINTS=2$). In this example, each integration has 4 groups ($NGROUPS=4$), and each group is composed of 8 frames (i.e. non-destructive reads). Within all but the last group in an integrations, 4 frames are marked for storage ($NFRAMES=4$) and 4 frames are discarded ($GROUPGAP=4$). In the final group in an integration, the detector is reset rather than performing the final $GROUPGAP$ samples of the detector (resulting in higher efficiency and reducing possible saturation and resulting latent images).

where $NCOL$ and $NROW$ define the dimensions of the subarray that is configured (including full array), and $10 \mu\text{sec}$ is the pixel addressing clock period. $Noutput$ refers to the number of output channels used, and is 4 in full-frame mode (i.e. $NCOLS = NROWS = 2048$), and is generally 1 for subarrays. (Subarrays with $NCOLS = 2048$ can be configured to use 4 output channels (this is known as *stripe-mode*), and will be supported, e.g. for NIRC*am* grism observations of point sources.) These complexities aside, frame times can be approximated as the total number of pixels being used ($NCOLS \times NROWS$) times 10

μsec . In full-frame mode this gives a frame time of 10.49 seconds (compared to the actual value of 10.74 seconds); for 320^2 and 64^2 subarrays the approximate and actual frame times are 1.02 and 1.07 seconds (320^2) and 41 and 49 msec (64^2).

MIRI subarrays work differently. All four outputs are always used, including for subarrays. However, the the lack of a hardware window mode (which the H2RG detectors do have) means that time must be spent clocking past the unused rows. As a result, the frame time for MIRI subarrays depend both on the size and location of the subarray, as follows:

$$T_{Frame} = \left(\left(\frac{SCOL + NCOL - 1}{4} + 10 \right) \times NROW + (1024 - NROW) \times 7 \right) \times 10\mu\text{sec}$$

where $SCOL$ is the starting column of the subarray. The overhead required to clock past the unused rows leads to a lower limit of 70 ms for a 1x1 subarray.

Term	Definition
Frame	Single non-destructive read performed during an integration.
Tframe	The time required to read all of the pixels on a detector (or within a subarray).
Group	A series of <i>frames</i> , some of which are stored, and some of which may be discarded.
NFRAMES	Number of <i>frames</i> in a <i>group</i> to store and downlink. NFRAMES must be a power of 2. If NFRAMES > 1 the frames are coadded before being stored.
GROUPGAP	Number of <i>frames</i> in a <i>group</i> to discard. The total number of <i>frames</i> within a <i>group</i> is NFRAMES + GROUPGAP.
NGROUPS	The number of <i>groups</i> within a single <i>integration</i> .
Tgroup	The time to perform all of the reads in a single <i>group</i> , equal to Tframe × (NFRAMES+GROUPGAP).
Integration	Single up-the-ramp set of samples of the pixels of a detector or within a subarray. Each integration is preceded by a reset. NGROUPS samples are stored and downlink for conversion to slope images by the ground system.

Table 9: MULTIACCUM exposure parameters (ALL CAPS) and related quantities.

Term	Definition
NINTS	The number of consecutive <i>integrations</i> within an <i>exposure</i> . For NIRC <i>am</i> , NIRISS, and NIRSpec, NINTS can not exceed 65535.
Integration Time	The duration of a single up-the-ramp <i>integration</i> , equal to the time between the <i>reset</i> at the beginning of the integration and the time of the final (saved) <i>frame</i> in the last <i>group</i> of the <i>integration</i> .
Exposure	A series of one or more <i>integrations</i> acquired without interruption.
Exposure Time	The total time spent collecting signal during an exposure, equal to $NINT \times Integration\ Time$
Exposure Duration	The total time spent executing and exposure, including resets and GROUPGAP frames. Equal to $tframe \times (NFRAME+GROUPGAP+1) \times NINTS$.

Table 9: JWST MULTIACCUM exposure definitions (continued).

C. Illustrative Science Programs

To illustrate the power of JWST’s instruments we have selected potential targets for observation, choosing either a primary transit, a secondary eclipse, or a full phase curve. Table Appendix 3) lists some of the properties of the planetary systems and Table Appendix 4 gives a representative observing program including integration times. To these times must be added a significant amount of overhead for slew taxes, telescope acquisition and instrument setup times.

Table Appendix 3. Illustrative *JWST* Target Stars

Star Name	Spec Type	K (mag)	Rp (R_{Jup})	Depth (ppm)	Period (day)	Transit Dur ¹ (hr)	Teff (K)
GJ436	M1	6.1	0.38	7,000	2.6	1	700
Gliese1214	M4.5	8.8	0.20	13,000	1.6	1	550
HD189733	G0	5.5	1.14	24,000	2.2	2	1200
HD209458	F8	6.3	1.38	14,00	3.5	3	1450
HD80606	G5	7.3	0.98	10,600	111	60	400-1500
Kepler-7	G1	11.5	1.50	6,800	4.9	120	1400
KOI-02311.01	G2	11.0	0.10	100	192	5	310
Sample TESS Target ²	M2	7.5	0.13	800	30	3	300

Note. — ¹Observation is $3\times$ the transit duration to account for time to measure the star before and after the transit/eclipse. For HD 80606 and Kepler-7 the duration is that required to observe a phase curve.¹ Illustrative properties of a nearby M dwarf that *TESS* might discover to have a Habitable Zone Super Earth.

The following notes pertain to Table Appendix 4 and give details of the instrument setup and SNR calculations.

1. Observed events are either a transit (Tr), secondary eclipse (SE), or a partial phase curve (PC).
2. SNR values given are for measuring either a single transit, the continuum day-side emission at eclipse, or the continuum emission for 1 hour of a phase curve using the system parameters in Table Appendix 3 unless otherwise specified. Actual time spent observing a transit or eclipse will be $\sim 3\times$ the transit duration for sufficient time on the star+planet as well as the star alone. Spectral SNRs are for the indicated event at the indicated resolution. SNRs for expected spectral or temporal features must be scaled from these single event values.
3. GJ 436 exceeds the NIRCcam imaging bright limit. SNR calculated for a NIRCcam grism + F356W filter observation of 1 secondary eclipse with all spectral information co-added.
4. NIRISS GJ 1214 transit spectrum SNR calculated for $\lambda = 0.6\text{to}2.7\mu\text{m}$ and $R=700$. See Figure 21a.
5. NIRCcam GJ 1214 transit spectrum SNR calculated for $\lambda = 3.22\mu\text{m}$ and $R=1000$. SNR improves with $R^{-0.5}$ if binned down further.
6. NIRCcam HD 189733 secondary eclipse spectrum SNR calculated for $\lambda = 3.56\mu\text{m}$ and $R=1000$. SNR improves with $R^{-0.5}$ if binned down further.
7. NIRISS HD 189733 primary transit SNR calculated for $\lambda = 3.6\mu\text{m}$ and $R=700$. See Figure 21b.

8. NIRCcam HD 80606 b phase curve SNR calculated for planet temperature of 1000 K. HD 80606 exceeds the NIRCcam imaging bright limit. SNR calculated for a NIRCcam grism + F444W filter with all spectral information co-added.
9. MIRI HD 80606 b secondary eclipse SNR calculated for planet temperature of 1400 K at $\lambda = 8.0\mu\text{m}$ and $R=100$ for 1 hour before eclipse.
10. Kepler-7b MIRI Silicate phase curve SNR calculated for $\lambda = 10.0\mu\text{m}$ and $R=3000$. SNR may improve as much as $R^{-0.5}$ if binned down to lower R . Beware that full spectral coverage requires 3 exposures with different dichroic / grating settings.
11. KOI-02311.01 NIRCcam transit spectrum SNR calculated for $\lambda = 3.22\mu\text{m}$ and $R=1000$. SNR improves with $R^{-0.5}$ if binned down further (SNR = 110 at $R=100$).
12. All NIRCcam calculations assume a systematic noise floor of 10 ppm per spectral / spatial resolution element per transit or eclipse event. NIRCcam phase curve observation SNRs are calculated for 1 hr during a phase curve that also covers 1 hr of secondary eclipse.
13. All MIRI calculations assume a systematic noise floor of 40 ppm per spectral / spatial resolution element per transit or eclipse event. MIRI phase curve observations SNRs are calculated for 1 hr during a phase curve that also covers 1 hr of secondary eclipse.
14. SNR expressed as a relative noise level in parts-per-million (ppm of the signal from the parent star). All calculations assume a minimum achievable noise level (systematic noise floor) of 20 ppm similar to what has been achieved in the best cases with HST. Note that the capability of NIRSpec to reach such low levels of systematics will only be demonstrated once in orbit. All numbers are given per spectral pixel (no spectral binning; see the spectral resolution curves in Fig. 15) and assuming the transit durations listed in Table 3 (with 2 times the transit duration spent out of transit or

eclipse). For (spectroscopic) phase curve observations, we have assumed that up to 1 hour of observation could be added for each point of the curve. To maximise the efficiency of the observations, we have allowed the use of integrations with a single frame readout ("*RESET-READ*" pattern, see discussion in Section 6.3) whenever relevant.

Source Name	Science Driver	Instrument Mode	Disperser/Filter	λ (μm)	Resh	Event ¹	SNR (or Noise) ² (1 Event)
GJ 436	Hot Neptune Dayside Map	NIRcam Imaging	F356W	3.11-4	4	SE	8.9 ³
GJ 1214	Sub-Neptune Flux	MIRI Imaging	F1000W	9-11	5	SE	7.0
	Sub-Neptune Spectrum	NIRISS Grism	GR700XD	0.6-2.3	300-800	Tr	75-100 ⁴
	Sub-Neptune Spectrum	NIRcam Grism	F322W2	2.4-4.0	1100-1700	Tr	55 ⁵
HD189733	Emission Spectrum	NIRcam Grism	F356W	3.15-3.97	~1500	SE	21 ⁶
	Transmission Spectrum	NIRISS Grism	GR700XD	1.10-2.70	~700	Tr	425 ⁷
	Tomographic imaging	MIRI Imaging	F770W	6.6-8.8	3.5	SE	33
	Tomographic spectro-imaging	NIRSpec	G140M/F170LP	1.7-3.1	700-1300	PC	100-250 ppm ¹⁴
HD209458	Tomographic imaging	NIRcam Imaging	F200W+WL	1.75-2.25	4	SE	80
HD80606	Periastron light curve	NIRcam Imaging	F444W	3.89-5	4	PC	22 ⁸
	Emission Spectrum	MIRI Imager	Fism	5-12	40-200	SE	12 ⁹
	Emission Spectrum (high res)	NIRSpec	G140H/F070LP	0.7-1.2	1300-2300	SE	100-20 ppm ¹⁴
			G140H/F100LP	1.0-1.8	1900-3600	SE	20-35 ppm ¹⁴
			G235M/F170LP	1.7-3.1	1900-3600	SE	20-50 ppm ¹⁴
			G395H/F290LP	2.9-5.2	1900-3600	SE	30-80 ppm ¹⁴
Kepler-7	Silicate Cloud Phase Curve	NIRcam Imaging	F444W	3.89 - 5	4	PC	9.5
	Silicate Cloud Phase curve	MIRI MRS/Ch2	Ch2	7- 12	3000	PC	0.3 ¹⁰
KOI-02311.01	Confirmation	NIRcam Imaging	F200W	1.75-2.25	4	Tr	5
TESS-001	Super Earth	NIRcam Grism	F322W2	2.42-4.01	1100-1700	Tr	35 ¹¹
	Super Earth	MIRI Imager	F1280W	11.6-14.0	5.3	SE	0.1
	Super Earth	NIRSpec	G140M/F070LP	0.7-1.2	500-850	Tr	1000-80 ppm ¹⁴
			G140M/F100LP	1.0-1.8	700-1300	Tr	60-100 ppm ¹⁴
			G235M/F170LP	1.7-3.1	700-1300	Tr	70-160 ppm ¹⁴
			G395M/F290LP	2.9-5.2	700-1300	Tr	90-200 ppm ¹⁴

Table Appendix 4: Description of illustrative programs

REFERENCES

- Angerhausen, D., Krabbe, A., & Iserlohe, C. 2006, in Society of Photo-Optical Instrumentation Engineers (SPIE) Conference Series, Vol. 6269, Society of Photo-Optical Instrumentation Engineers (SPIE) Conference Series
- Artigau, É., Donati, J.-F., & Delfosse, X. 2011, in Astronomical Society of the Pacific Conference Series, Vol. 448, 16th Cambridge Workshop on Cool Stars, Stellar Systems, and the Sun, ed. C. Johns-Krull, M. K. Browning, & A. A. West, 771
- Bakos, G. Á., Hartman, J. D., Torres, G., et al. 2011, European Physical Journal Web of Conferences, 11, 1002
- Ballard, S., Fabrycky, D., Fressin, F., et al. 2011, ApJ, 743, 200
- Batalha, N., Kalirai, J. S., Lunine, J. I., & Mandell, A. 2014, American Astronomical Society Meeting Abstracts, 223, #325.03
- Bean, J. L., Seifahrt, A., Hartman, H., et al. 2010, ApJ, 713, 410
- Berta, Z. K., Irwin, J., Charbonneau, D., Burke, C. J., & Falco, E. E. 2012, AJ, 144, 145
- Berta, Z. K., Charbonneau, D., Désert, J.-M., et al. 2012, ApJ, 747, 35
- Boccaletti, A., Lagage, P.-O., Baudoz, P. et al. 2014, PASP, submitted
- Bouchet, P., Garcia-Marin, M., Lagage, P.-O., et al. 2014, PASP, submitted
- Broeg, C., Fortier, A., Ehrenreich, D., et al. 2013, in European Physical Journal Web of Conferences, Vol. 47, European Physical Journal Web of Conferences, 3005
- Brown, T. M. 2003, ApJ, 593, L125
- Burke, C. J., Bryson, S. T., Mullally, F., et al. 2014, ApJS, 210, 19

- Charbonneau, D., Berta, Z. K., Irwin, J., et al. 2009, *Nature*, 462, 891
- Clanton, C., Beichman, C., Vasisht, G., Smith, R., & Gaudi, B. S. 2012, *PASP*, 124, 700
- Cowan, N. B., & Agol, E. 2008, *ApJ*, 678, L129
- Croll, B., Lafreniere, D., Albert, L., et al. 2011, *AJ*, 141, 30
- Crossfield, I. J. M., Hansen, B. M. S., Harrington, J., et al. 2010, *ApJ*, 723, 1436
- Crossfield, I. J. M., Knutson, H., Fortney, J., et al. 2012, *ApJ*, 752, 81
- Dawson, R. I., Johnson, J. A., Fabrycky, D. C., et al. 2014, *ApJ*, 791, 89
- Deming, D., Wilkins, A., McCullough, P., et al. 2013, *ApJ*, 774, 95
- Demory, B.-O., Gillon, M., Seager, S., et al. 2012, *ApJ*, 751, L28
- de Wit, J., Gillon, M., Demory, B.-O., & Seager, S. 2012a, *A&A*, 548, A128
- . 2012b, *A&A*, 548, A128
- Deming, D., Seager, S., Winn, J., et al. 2009, *PASP*, 121, 952
- Dittmann, J. A., Irwin, J. M., Charbonneau, D., & Berta-Thompson, Z. K. 2014, *ApJ*, 784, 156
- Dressing, C. D., & Charbonneau, D. 2013, *ApJ*, 767, 95
- Dressing, C. D., & Charbonneau, D. 2013, *ApJ*, 767, 95
- Eastman, J., Siverd, R., & Gaudi, B. S. 2010, *PASP*, 122, 935
- Ferruit, P., Bagnasco, G., Barho, R., et al. 2012, The JWST near-infrared spectrograph NIRSpec: status, doi:10.1117/12.925810

- Foreman-Mackey, D., Hogg, D. W., & Morton, T. D. 2014, *ApJ*, 795, 64
- Fortney, J. J., Mordasini, C., Nettelmann, N., et al. 2013, *ApJ*, 775, 80
- Fraine, J. D., Deming, D., Gillon, M., et al. 2013, *ApJ*, 765, 127
- Fraine, J. D., Deming, D., Gillon, M., et al. 2013, *ApJ*, 765, 127
- Fressin, F., Torres, G., Charbonneau, D., et al. 2013, *ApJ*, 766, 81
- Gersch-Range, J. and Perrin, M. 2014, *Journal of Astronomical Telescopes, Instruments, and Systems*, 1,1.
- Gillett, F. C., Low, F. J., & Stein, W. A. 1969, *ApJ*, 157, 925
- Gillon, M., Jehin, E., Delrez, L., et al. 2013, in *Protostars and Planets VI*, Heidelberg, July 15-20, 2013. Poster #2K066, 66
- Gillon, M., Demory, B.-O., Madhusudhan, N., et al. 2014, *A&A*, 563, A21
- Glasse, A., Rieke, G., Bauwens, E. et al. 2014, *PASP*, submitted
- Guillot, T., Burrows, A., Hubbard, W. B., Lunine, J. I., & Saumon, D. 1996, *ApJ*, 459, L35
- Hansen, C. J., Schwartz, J. C., & Cowan, N. B. 2014, arXiv:1402.6699
- Henry, T. J., Jao, W.-C., Subasavage, J. P., et al. 2006, *AJ*, 132, 2360
- Howard, A. W., Sanchis-Ojeda, R., Marcy, G. W., et al. 2013, *Nature*, 503, 381
- Howell, S. B., Sobeck, C., Haas, M., et al. 2014, arXiv:1402.5163
- Howell, S. B., Sobeck, C., Haas, M., et al. 2014, ArXiv e-prints, arXiv:1402.5163
- Huitson, C. M., Sing, D. K., Pont, F., et al. 2013, *MNRAS*, 434, 3252

- Kaltenegger, L., & Traub, W. A. 2009, *ApJ*, 698, 519
- Kasting, J. F., Whitmire, D. P., & Reynolds, R. T. 1993, *Icarus*, 101, 108
- Kirkpatrick, J. D., Reid, I. N., Liebert, J., et al. 1999, *ApJ*, 519, 802
- Kendrew, S., Scheithauer, S., Bouchet, P. et al. 2014, *PASP*, submitted
- Konopacky, Q. M., Barman, T. S., Macintosh, B. A., & Marois, C. 2013, *Science*, 339, 1398
- Knutson, H. A., Charbonneau, D., Allen, L. E., et al. 2007, *Nature*, 447, 183
- Knutson, H. A., Charbonneau, D., Cowan, N. B., et al. 2009, *ApJ*, 703, 769
- Knutson, H. A., Lewis, N., Fortney, J. J., et al. 2012, *ApJ*, 754, 22
- Knutson, H. A., Benneke, B., Deming, D., & Homeier, D. 2014, *Nature*, 505, 66
- Kreidberg, L., Bean, J. L., Désert, J.-M., et al. 2014, *Nature*, 505, 69
- Kreidberg, L., Bean, J. L., Désert, J.-M., et al. 2014, *Nature*, 505, 69
- Lee, J.-M., Fletcher, L. N., & Irwin, P. G. J. 2012, *MNRAS*, 420, 170
- Lépine, S. 2005, *AJ*, 130, 1680
- Line, M. R., & Yung, Y. L. 2013, *ApJ*, 779, 3
- Lissauer, J. J., Jontof-Hutter, D., Rowe, J. F., et al. 2013, *ApJ*, 770, 131
- Mandell, A. M., Haynes, K., Sinukoff, E., et al. 2013, *ApJ*, 779, 128
- Mahadevan, S., Ramsey, L., Wright, J., et al. 2010, in *Society of Photo-Optical Instrumentation Engineers (SPIE) Conference Series*, Vol. 7735, *Society of Photo-Optical Instrumentation Engineers (SPIE) Conference Series*

- Majeau, C., Agol, E., & Cowan, N. B. 2012a, *ApJ*, 747, L20
- . 2012b, *ApJ*, 747, L20
- Madhusudhan, N., Knutson, H., Fortney, J., & Barman, T. 2014, arXiv:1402.1169 (accepted for *Protostars and Planets VI*).
- Menou, K., Cho, J. Y.-K., Seager, S., & Hansen, B. M. S. 2003, *ApJ*, 587, L113
- Morley, C. V., Marley, M. S., Fortney, J. J., et al. 2014, *ApJ*, 787, 78
- Nutzman, P., & Charbonneau, D. 2008, *PASP*, 120, 317
- Öberg, K. I., Murray-Clay, R., & Bergin, E. A. 2011, *ApJ*, 743, L16
- Perryman, M. A. C., Lindegren, L., Kovalevsky, J., et al. 1997, *A&A*, 323, L49
- Perryman, M. A. C., de Boer, K. S., Gilmore, G., et al. 2001, *A&A*, 369, 339
- Petigura, E. A., Marcy, G. W., & Howard, A. W. 2013, *ApJ*, 770, 69
- Petigura, E. A., Howard, A. W., & Marcy, G. W. 2013, *Proceedings of the National Academy of Science*, 110, 19273
- Pont, F., Sing, D. K., Gibson, N. P., et al. 2013, *MNRAS*, 432, 2917
- Quirrenbach, A., Amado, P. J., Seifert, W., et al. 2012, in *Society of Photo-Optical Instrumentation Engineers (SPIE) Conference Series*, Vol. 8446, *Society of Photo-Optical Instrumentation Engineers (SPIE) Conference Series*
- Ricker, G. R., Winn, J. N., Vanderspek, R., et al. 2014, arXiv:1406.0151, submitted to *SPIE*.
- Rieke, G., Ressler, M. E., Morrison, J. E. et al. 2014, *PASP*, submitted

- Rieke, G. H., Young, E. T., Cadien, J., et al. 2004, in Presented at the Society of Photo-Optical Instrumentation Engineers (SPIE) Conference, Vol. 5487, Society of Photo-Optical Instrumentation Engineers (SPIE) Conference Series, ed. J. C. Mather, 5061
- Rogers, L. A., & Seager, S. 2010, *ApJ*, 716, 1208
- Seager, S., & Deming, D. 2009, *ApJ*, 703, 1884
- Shabram, M., Fortney, J. J., Greene, T. P., & Freedman, R. S. 2011, *ApJ*, 727, 65
- Siverd, R. J., Pepper, J., Stanek, K., et al. 2009, *IAU Symposium*, 253, 350
- Sozzetti, A., Bernagozzi, A., Bertolini, E., et al. 2013, in *European Physical Journal Web of Conferences*, Vol. 47, *European Physical Journal Web of Conferences*, 3006
- Snellen, I. A. G., Stuik, R., Navarro, R., et al. 2012, *Proc. SPIE*, 8444,
- Stevenson, K. B., Harrington, J., Fortney, J. J., et al. 2012, *ApJ*, 754, 136
- Stevenson, K. B., Harrington, J., Lust, N. B., et al. 2012, *ApJ*, 755, 9
- Sullivan, P., Winn, J. N., Dressing, C. D., et al. 2014, *American Astronomical Society Meeting Abstracts*, 224, #113.03
- van Altena, W. F., Lee, J. T., & Hoffleit, D. 1995, *VizieR Online Data Catalog*, 1174, 0
- Wells, M., Pel, J.-W., Glasse, A. et al. 2014, *PASP*, submitted
- Williams, P. K. G., Charbonneau, D., Cooper, C. S., Showman, A. P., & Fortney, J. J. 2006, *ApJ*, 649, 1020

Young, E. T., Rieke, G. H., Cadien, J., et al. 2003, in Society of Photo-Optical Instrumentation Engineers (SPIE) Conference Series, Vol. 4850, Society of Photo-Optical Instrumentation Engineers (SPIE) Conference Series, ed. J. C. Mather, 98–107